

# UC San Diego

## UC San Diego Electronic Theses and Dissertations

### Title

Electromagnetic analysis of nanostructure dispersion in polymer matrices

### Permalink

<https://escholarship.org/uc/item/48d2x5qv>

### Authors

Pfeifer, Steven Charles

Pfeifer, Steven Charles

### Publication Date

2012

Peer reviewed|Thesis/dissertation

UNIVERSITY OF CALIFORNIA, SAN DIEGO

Electromagnetic Analysis of Nanostructure Dispersion in Polymer  
Matrices

A dissertation submitted in partial satisfaction of the  
requirements for the degree Doctor of Philosophy  
in  
Materials Science and Engineering

by

Steven Charles Pfeifer

Committee in charge:

Professor Prabhakar R. Bandaru, Chair  
Professor Pao C. Chau  
Professor Vlado A. Lubarda  
Professor Vitali F. Nesterenko  
Professor Jason R. Schweinsberg

2012

Copyright

Steven Charles Pfeifer, 2012

All rights reserved.

The dissertation of Steven Charles Pfeifer is approved, and it is acceptable in quality and form for publication on microfilm and electronically:

---

---

---

---

---

Chair

University of California, San Diego

2012

*Dedicated*

*to*

*My parents*

# Table of Contents

Signature Page.....	iii
Dedication Page.....	iv
Table of Contents.....	v
List of Figures.....	vii
List of Tables.....	viii
Acknowledgement.....	ix
Curriculum Vita.....	xi
Abstract of the Dissertation.....	xii
<b>Chapter 1. Introduction.....</b>	<b>1</b>
1.1 Interphase.....	2
1.2 Percolation Threshold with Random CNT Lengths.....	3
1.3 Characterizing CNT Dispersion in Nanocomposites.....	8
1.4 Modeling the Electrical Impedance of Nanocomposites.....	11
<b>Chapter 2. Analysis of electrical percolation thresholds in carbon nanotube networks, using the Weibull probability distribution ...</b>	<b>16</b>
2.1 Introduction.....	16
2.2 The Stochastic Percolation Model.....	16
2.3 Experimental.....	20
2.4 Conclusion.....	25

<b>Chapter 3. A method for quantitatively characterizing the dispersion of nanostructures in polymers ...</b>	<b>27</b>
3.1 Introduction.....	27
3.2 Principles of the Approach.....	28
3.3 Implementation of the $\langle d(P  Q) \rangle$ metric to gauge the uniformity of a given CNT distribution within a polymer matrix .....	30
3.4 Conclusion.....	37
<b>Chapter 4. A comparison of models for determining the relative permittivity of nanotube constituted polymer composites .....</b>	<b>44</b>
4.1 Introduction.....	44
4.2 Experimental Procedures.....	45
4.3 Electrical Impedance Model.....	50
4.4 Discussion.....	52
4.5 Conclusion.....	53
<b>Chapter 5. Summary of dissertation.....</b>	<b>55</b>
<b>References.....</b>	<b>58</b>

## List of figures

Figure 1-1 Interphase for micron size particles and nanometric particles.....	4
Figure 1-2 This figure illustrates the concept of an excluded volume using a two-dimensional view .....	6
Figure 1-3 (based on figure 32 in [9]) Example of a percolation power law curve showing a sudden jump in DC conductivity at the critical CNT volume fraction $\phi_c$ demarcating the creation of a CNT percolation network. ....	7
Figure 1-4 The use of the $d$ -metric to study the evolution in contrast.....	10
Figure 2-1 The theoretical variation of the critical percolation threshold ( $\phi_c$ ) plotted as a function of the CNT aspect ratio assuming a deterministic length and diameter.....	19
Figure 2-2 The lengths of (a) SWCNTs, and (b) MWCNTs dispersed into the polymer matrix in the present study, and (c) MWCNTs from another study in literature [1] (Yu et al, Science, 287, 637 – 640, 2000), plotted on Weibull probability paper.....	22
Figure 2-3 The variation of the DC electrical conductivity ( $\sigma_{DC}$ ) with volume fraction ( $\phi$ ) for (a) SWCNTs and (b) MWCNTs dispersed in a polymer matrix, was used to determine the percolation threshold ( $\phi_c$ ). ....	25
Figure 3-1 The uniformity of dispersion of carbon nanotubes (CNTs) dispersed in a RET polymer matrix, decreases from the top to the bottom in these Scanning Electron Microscope (SEM) micrographs .....	38
Figure 4-1 Variation of Relative Permittivity with Frequency and CNT Filler Concentration.....	47
Figure 4-2 The variation of electrical impedance ( $Z^*$ ) with frequency .....	48
Figure 4-3 Equivalent circuit models for (a) an equivalent series resistance model and (b) the two-dimensional resistor – capacitor model (2D RC).....	49

## List of tables

- Table 1-1 The evolution of the  $d$ -metric with incremental, single-pixel departures from a uniform distribution. In the pattern legend,  $I_x$ ,  $x$  indicates the number of white pixels, and  $d(\text{UNIFORM} \parallel I_0) = 0$ .....11
- Table 3-1 The  $d$ -metric for the images of Figure 3-1, indicate a quantification of the degree/uniformity of dispersion. While the numbers in **bold** indicate the  $d$ -metric values, the standard deviation from ten measurements is indicated in the brackets.....41
- Table 3-2 The  $d$ -metric for the images in Figure 3-2, indicate a quantification of the degree/uniformity of dispersion. While the numbers in **bold** indicate the  $d$ -metric values, the standard deviation from ten measurements is indicated in the brackets....42
- Table 3-3 The  $d$ -metric for the images in Figure 3-3, indicate a quantification of the degree/uniformity of dispersion. While the numbers in **bold** indicate the  $d$ -metric values, the standard deviation from ten measurements is indicated in the brackets....43

## Acknowledgement

I wish to sincerely thank my advisor, Professor Prabhakar R.

Bandaru, for his insight, support, creativity, and guidance during the course of this research. I wish to express my sincere gratitude to my committee members for their time and helpful discussions: Professor Prabhakar R. Bandaru, Chair; Professor Pao C. Chau; Professor Vlado A. Lubarda; Professor Vitali F. Nesterenko; and Professor Jason R. Schweinsberg.

Chapter 2, in full, has been published in the *Journal of Applied Physics*, **108** 024305 (2010) “Analysis of electrical percolation thresholds in carbon nanotube networks using the Weibull probability distribution” by S. Pfeifer, S. H. Park, and P. R. Bandaru. This paper was selected for republication in the *Virtual Journal of Nanoscale Science & Technology*, (July, 2010). Chapter 3, in full, has been submitted for publication in *Nanotechnology* “A method for quantitatively characterizing the dispersion of nanostructures in polymer composites” by S. Pfeifer and P. R. Bandaru. Chapter 4, in full, has been submitted to the *Journal of Applied Physics* “A comparison of models for determining the relative permittivity of nanotube constituted polymer composites” by S. Pfeifer, S. H. Park, and P. R. Bandaru. (2012).

Many thanks to those who met with me to discuss various aspects of this work: Professor Jack Wolf, Professor Tara Javidi, Professor Massimo Franceschetti, Dr. Sunghoon Park, Ryan Anderson, Rahul Kapadia and Byung-wook Kim.

Special thanks go to Charlotte Lauve for taking care of the administrative burdens for me.

I wish to thank my employer General Atomics Aeronautical, Inc. for all their assistance and consideration.

**Steven Charles Pfeifer**

La Jolla, August 2012

# Curriculum Vita

## Education

1982 B.S., Chemical Engineering

University of California San Diego, United States

2005 M.Eng., Electrical and Computer Engineering

University of California San Diego, United States

2012 Ph.D., Materials Science and Engineering

University of California San Diego, United States

## JOURNAL PUBLICATIONS:

Steven Pfeifer, Sung-Hoon Park, and Prabhakar R. Bandaru, “Analysis of electrical percolation thresholds in carbon nanotube networks using the Weibull probability distribution”, *Journal of Applied Physics*, 108: 024305, 2010.

This paper was selected for republication in the *Virtual Journal of Nanoscale Science & Technology (Carbon Nanotubes, C60, and Related Studies)*, vol. 22, issue 5, August 2, 2010.

Steven Pfeifer and Prabhakar R. Bandaru, “A method for quantitatively characterizing the dispersion of nanostructures in polymers”, (submitted to *Nanotechnology*).

Steven Pfeifer, Sung-Hoon Park, and Prabhakar R. Bandaru, “A comparison of models for determining the relative permittivity of nanotube constituted polymer composites”, (submitted to the *Journal of Applied Physics*).

# **ABSTRACT OF THE DISSERTATION**

Electromagnetic Analysis of Nanostructure Dispersion in Polymer Matrices

By

Steven Charles Pfeifer

Doctor of Philosophy in Materials Science and Engineering

University of California, San Diego, 2012

Professor Prabhakar R. Bandaru, Chair

A method is proposed for determining electrical percolation thresholds in carbon nanotube (CNT) networks when CNT lengths vary randomly. The random distribution in CNT lengths, commonly observed in practical processing and dispersion, was confirmed to be of the Weibull type. Nanocomposites consisting of both single- and multi-walled CNTs dispersed in reactive ethylene terpolymer were synthesized and the projected theoretical CNT volume concentrations required for electrical percolation were shown to closely correspond to the experimentally determined values.

A metric for quantifying the degree of dispersion of nanostructures in polymers, based on information theory, is also suggested. The uniform dispersion of nanoparticles in polymer-based composites enhances material properties such as

structural reinforcement, electromagnetic interference shielding, etc. The proposed measure of dispersion uses a quadrat-based sampling algorithm and the average Kullback-Leibler divergence is used to correlate randomness to the dispersion. This allows a quantitative comparison of cross-sectional images of nanostructure networks with different degrees of dispersion in a polymer.

Finally, the complex electrical impedances of the nanocomposites were evaluated at different CNT aspect ratios and volume fractions in the 80 MHz – 500 MHz frequency range. The electrical impedances were fit to an equivalent-series resistance (ESR) circuit model, and compared with distributed electrical models such as an RC network and constant phase element representations. Dielectric permittivity measurements demonstrate that the constant phase element model, which corresponds to a distribution/dispersion of relaxation times, best fits the electrical response of the composites.

## Chapter 1. Introduction

Nanocomposites (NCs) consisting of carbon nanotubes (CNTs) dispersed in a polymer have exhibited novel electrical characteristics including enhanced electromagnetic shielding,[2] heightened infrared photoresponse,[3] and low electrical percolation thresholds.[4] Nanoparticle-polymer NCs also have been identified with superior breakdown strength and very high density charge storage superior to that afforded by using micrometer particles with the same material composition.[5]

These properties arise from the nanometric size of the minority phase and the uniformity of the nanostructures' dispersal within the polymer matrix. Properties of CNT-based NCs of technological interest arise from the high CNT aspect ratio  $AR = \frac{CNT\ length}{CNT\ diameter}$ . Chapter 2 of this thesis shows how a large CNT aspect ratio results in electrical percolation at low CNT volume fractions. Many key NC properties also depend on the uniformity of their dispersal within the polymer matrix. Chapter 3 of this thesis provides an algorithm for characterizing the degree of dispersion of a minority phase in a majority phase. This algorithm also can be adapted to compare color or greyscale images for stereological, medical, or other applications. Chapter 4 develops an electrical impedance circuit model using permittivity measurements of

functionalized, multi-walled CNTs ester bonded to reactive ethylene terpolymer. It was determined that the electrical impedance fit a constant phase element.

## 1.1 Interphase

Nanoparticles can interact with the majority phase creating a new phase that extends in a zone  $\sim 10 - 20$  nm from each nanoparticle. This new phase, called *interphase*, has material properties different from the constituent phases. The exact nature of this interaction volume is the subject of ongoing study but its properties are measurably different from either constituent. The properties of interphase depend on how the nanoparticle interacts with the majority phase. An example: dielectric constants for some NCs have been measured that exceed constituent permittivities:  $\epsilon_{Polymer}' < \epsilon_{Particle}' < \epsilon_{NC}'$ . This is outside the  $\epsilon_{Polymer}' < \epsilon_{Composite}' < \epsilon_{particle}'$  bounds predicted by permittivity mixing equations such as those from Maxwell, Lichtenecker, etc. This finding is attributed to changes in space charge distribution in the interphase volume.[6] Chemical bonding between the polymer and nanostructures has been found to lower  $\epsilon_{NC}'$  in some cases, where the polymer chains become tethered and confined by the adjacent nanostructures. High electric breakdown strength and density charge storage also have been attributed to interphase where charge carrier scattering and changes in space charge distribution have been observed in the interaction zone between polymer and nanoparticle.[7] Most of the NC is interphase even at low inclusion volume fractions so the interphase properties can dominate the properties of the NC. Engineering the interphase to create new materials is of particular technological and scientific interest since.

Both nanoparticles and micron size inclusion have the same interphase volume of interaction extending in a zone  $\sim 10 - 20$  nm from each inclusion. With micron size inclusions the total volume fraction of interphase is a small part of the total composite volume because each micron inclusion is much larger than the interphase volume around the inclusion. In a composite with many such large inclusions, most of the volume is simply the phase of the majority constituent. This same  $10 - 20$  nm zone of interaction exists around each of the nanostructures in a NC. But in this case, the small size of the nanoparticles creates a large total volume fraction interphase. Even at low nanoparticle loadings, most of the NC volume is interphase because of the nanometer scale dimensions of the minority phase. This concept is illustrated in figure 1-1.

## **1.2 Percolation Threshold with Random CNT Lengths**

Interphase and low percolation thresholds depend on complete dispersion of the nanoinclusions. High van der Waals forces cause the nanostructures to “stick” together in clusters. Dispersion techniques such as ultrasonification can damage nanostructures and also lower CNT aspect ratio by destructively fracturing the CNTs. Lowered aspect ratios in turn increase the number of CNTs required to achieve electrical percolation. A lower CNT volume fraction is desirable to reduce cost and maintain NC flexibility, as polymer NCs can become brittle at high CNT loadings.

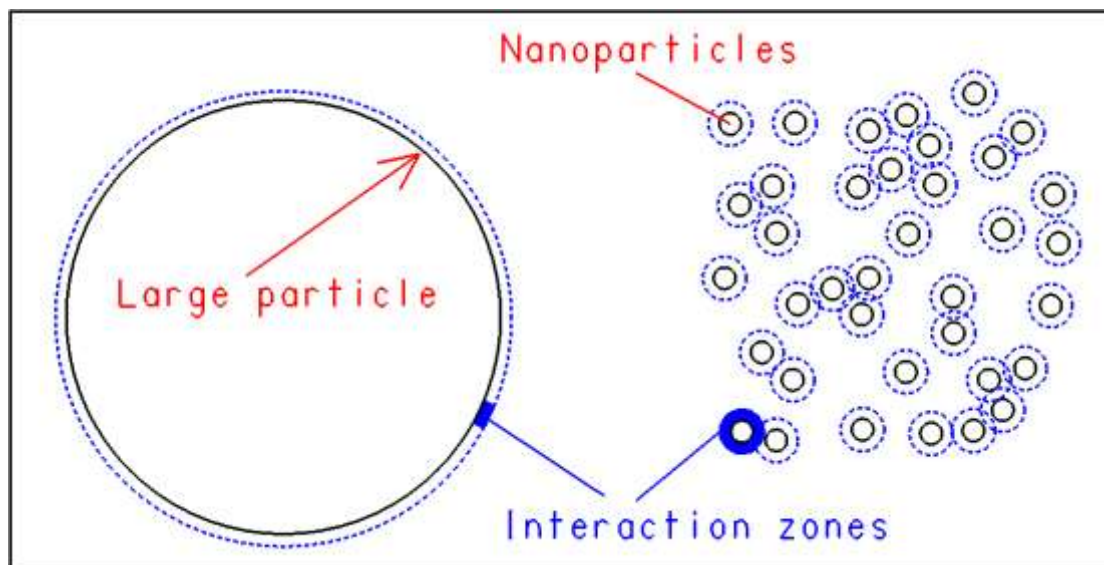


Figure 1-1 (not to scale): Interphase for micron size particles and nanometric particles. The dashed lines in blue font represent a  $\sim 10 - 20$  nm zone of interaction between inclusions shown as black circles and the adjacent polymer. Large (micron-size) inclusions interact with the polymer to make an interphase volume that comprises a small volume fraction of the total composite volume. With micron-size inclusions, most of the composite volume remains the polymer majority phase. The same  $10 - 20$  nm zone of interaction between nanometric inclusions is shown to the right of figure 1-1. The polymer results in a large volume fraction interphase that occupies most of the nanocomposite volume – even at low nanoparticle volume fractions.[8]

Chapter two uses an excluded volume approach to develop an equation for determining the minimum CNT volume fraction required to achieve electrical percolation when the CNT lengths vary randomly. The excluded volume (area) is the volume (area) around a CNT where the center of another CNT cannot enter without

overlapping.[9] Figure 1-2 illustrates the excluded volume concept using two dimensional views of the excluded area for various sized objects. In our study, CNTs are modeled as capped cylinders (spherocylinders) to simulate a cylinder of carbon molecules capped at either end by hemispherical buckyballs. The excluded volume for two CNTs modeled as capped cylinders is a capped parallelepiped (figure 1-2c).

Our theoretical equation for the percolation threshold considers a network of CNTs dispersed in a polymer/insulating matrix of unit volume. At the percolation threshold, the probability of not selecting any CNT (corresponding to a point in the matrix) is  $1 - \emptyset_C$ , where  $\emptyset_C$  is the critical CNT volume at percolation. Chapter two uses this result with the probability chain rule to relate  $\emptyset_C$  to the expected value (ensemble average) of the CNT volume and CNT excluded volume. Monte Carlo simulations show that the product of the CNT excluded volume with the number of CNTs at the percolation threshold is estimated as 1.4. This is an upper bound when the CNT lengths vary randomly, as the expected value of the excluded volume should be weighted to favor the longer CNTs. Substitution of the excluded volume for a capped parallelepiped gives the final result, for CNTs of diameter “D” and random length  $\underline{L}$ ,

$$\emptyset_C(\underline{L}) = \frac{1.4}{\frac{4\pi}{3}D^3 + 2\pi D^2 E[\underline{L}] + \frac{\pi}{2}DE[\underline{L}^2]} \left( \frac{\pi}{6}D^3 + \frac{\pi}{4}D^2 E[\underline{L}] \right)$$

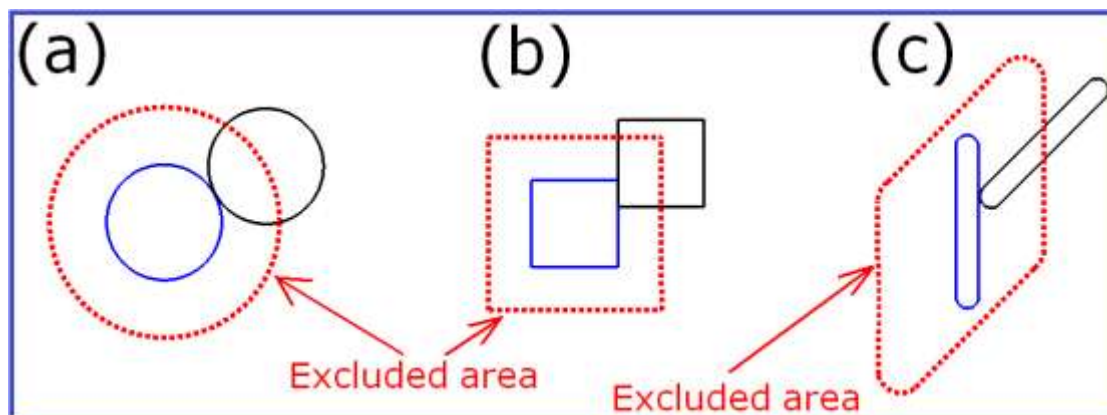


Figure 1-2 (not to scale): This figure illustrates the concept of an excluded volume using a two-dimensional view. The excluded area is the region enclosed by the center of one object (black font) contacting and moving around the periphery of another similar object (blue font). The excluded area is enclosed by the red dashed lines for various object shapes. The objects shown in (c) represent a two-dimensional view of CNTs. The excluded volume is the three-dimensional zone enclosed by the center of an object contacting and moving around (but never overlapping with) another similar object. For two CNTs modeled as spherocylinders (capped cylinders) the excluded volume would be a capped parallelepiped.

NC samples were tested at various CNT volume fractions. One set of NC samples used single-walled CNTs and another used multi-walled CNTs. All CNTs were functionalized so they would ester bond to the reactive ethylene terpolymer.

DC conductivity was measured on high resistivity (resistance  $> 1 \text{ G}\Omega$ ) NC samples using an Agilent B1500A semiconductor device analyzer with triaxial probes.

The data was fit to a power law to experimentally determine the critical percolation threshold (see figure 1-3). At the critical percolation threshold  $\phi_c$ , a jump in DC conductivity is evident and the data fits a percolation power law near and above  $\phi_c$ . The expected values of the random CNT lengths were established either using sample statistics or by fitting CNT lengths after ultrasonification to a Weibull probability distribution.

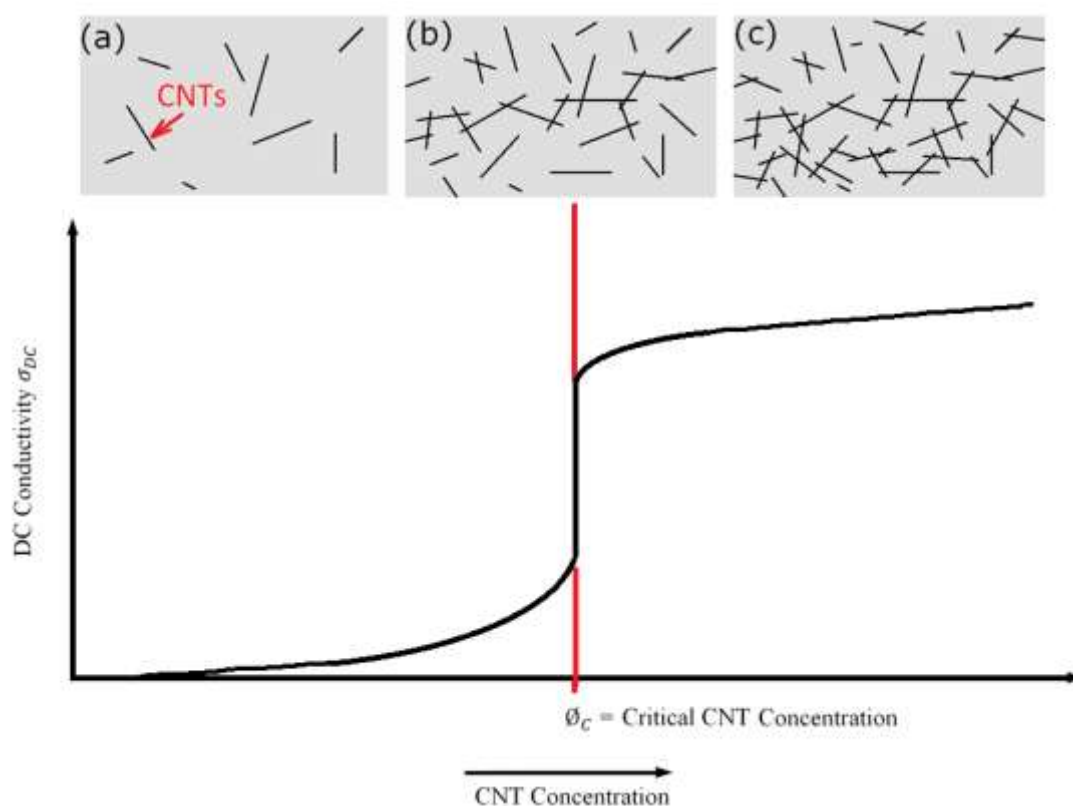


Figure 1-3 (based on figure 32 in [9]) Example of a percolation power law curve showing a sudden jump in DC conductivity at the critical CNT volume fraction  $\phi_c$  demarcating the creation of a CNT percolation network. The percolating CNT network causes the increase in DC conductivity[10].

Chapter two shows that our percolation equation closely agreed with our experimental measurements of the electrical percolation threshold. Our single-walled CNT NC had a theoretical percolation threshold of  $\varnothing_C \sim 0.00073$  which agrees with the experimentally measured threshold  $\varnothing_C \sim 0.011$ . Our multi-walled CNT NC had a theoretical percolation threshold of  $\varnothing_C \sim 0.0193$  which compares well to the experimental threshold  $\varnothing_C \sim 0.0147$ .

### **1.3 Characterizing CNT Dispersion in Nanocomposites**

Chapter three presents our algorithm for characterizing CNT dispersion in NCs. This algorithm is flexible in that transmission/scanning electron microscopy (TEM / SEM) images of a composite cross-section can be compared either to another image or to a probability distribution. Our algorithm superimposes 10,000 randomly-placed squares called *quadrats* over the micrograph. The large number of quadrat sampling allows the algorithm to be used with very large images. The number of pixels corresponding to CNTs within each quadrat are counted. The counts form a distribution which can be mathematically compared to another preferred (ideal) image or to a probability distribution.

The equation used for dispersion characterization measures the “distance” between the distribution corresponding to the image and another distribution. The equation is based on information theory, which is a foundation for modern digital image processing. Any image can be reconstructed using computer source code. The

smallest number of lines of binary source code required to reconstruct the image have been found to relate to the complexity of the image. One example: a snowflake or crystal is a fractal with a repeating base image and little randomness. Reconstruction of such an image requires a small number of lines of source code. Another example: very few lines of code are required to display  $\pi = 3.1415\dots$  to an arbitrary number of significant digits. But additional lines of code are required to reconstruct a random number to the same number of significant digits. As any image becomes less deterministic and instead exhibits more randomness, the minimum number of lines of binary computer code required to reconstruct the image increases. This concept is called a Kolmogorov complexity: any image's complexity can be described by the smallest number of lines of binary computer source code needed to characterize the object. The Kolmogorov complexity is approximately equal to information entropy, which is the expected value (ensemble average) of  $-\log [p(\underline{X})]$ , where  $p(\underline{X})$  is a probability mass function. It is surprising that the smallest number of lines of computer code is related to a probability, but it seems to follow from the viewpoint that a computer is a type of data decompressor.[11]

The distance between two distributions can be gauged by subtracting the informational entropy of "p" with probabilities  $p_i$  from another distribution "q"

estimated using probabilities  $q_i$ : 
$$- \left[ - \sum_{i=1}^n p_i \log_2(p_i) \right] - \sum_{i=1}^n p_i \log_2(q_i) \equiv D(p||q).$$

$D(p||q)$  does not always equal  $D(q||p)$ . Ideally a true dispersion metric should behave like a Euclidean distance. It should give the same distance when comparing

distribution “p” to distribution “q” as when comparing “q” to “p”. But  $D(p||q)$  lacks this type of symmetry since the order of the comparison usually changes the value of  $D(p||q)$ . We corrected this asymmetry by using the relation  $d(p||q) \equiv D(p||q) - D(q||p)$  as our dispersion equation. The “d-metric”  $d(p||q)$  provides the desired symmetry of a true distance metric in that  $d(p||q) = d(q||p)$  always holds when  $d(p||q)$  and  $d(q||p)$  are well-defined.

Our algorithm used  $d(p||q)$  to successfully distinguish between published images known to be severe tests of a dispersion algorithm. This is described in detail in chapter three of this thesis. Our algorithm also successfully detected single pixel deviations in a 1678 pixel X 1070 pixel size image (see figure 1-4 and table 1-1). The images were compared to a uniform probability distribution and the results presented in table 1-1.

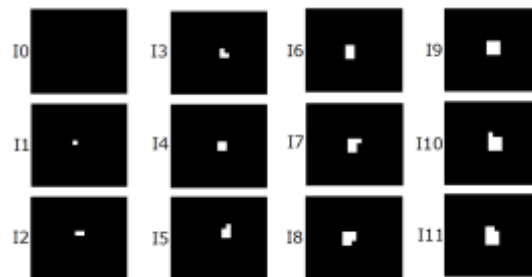


Figure 1-4: An example of the use of the proposed  $d$ -metric to study the evolution in contrast. The progressive increase in the number of white pixels (in the legend  $I_x$ ,  $x$  indicates the number of white pixels) results in an increase in the value of the  $d$ -metric (see table 1-1), which can be used as a measure of the deviation from a standard uniform probability distribution. The images indicate a magnified (800X) view of a part of a 1678 pixel X 1070 pixel size image.

**Table 1-1.** The evolution of the  $d$ -metric with incremental, single-pixel departures from a uniform distribution. In the pattern legend, Ix, x indicates the number of white pixels, and  $d(\text{UNIFORM} \parallel \text{I0}) = 0$

Pattern	No. of Light Pixels	$\langle d(\text{UNIFORM} \parallel \text{Pattern Name}) \rangle$	Standard Deviation
I0	0	0.0000	0
I1	1	$1.95 \cdot 10^{-10}$	$6.64 \cdot 10^{-11}$
I2	2	$8.07 \cdot 10^{-10}$	$2.48 \cdot 10^{-10}$
I3	3	$1.75 \cdot 10^{-9}$	$5.53 \cdot 10^{-10}$
I4	4	$2.88 \cdot 10^{-9}$	$8.94 \cdot 10^{-10}$
I5	5	$4.65 \cdot 10^{-9}$	$1.91 \cdot 10^{-9}$
I6	6	$7.67 \cdot 10^{-9}$	$1.70 \cdot 10^{-9}$
I7	7	$9.79 \cdot 10^{-9}$	$3.06 \cdot 10^{-9}$
I8	8	$1.12 \cdot 10^{-8}$	$3.43 \cdot 10^{-9}$
I9	9	$1.55 \cdot 10^{-8}$	$3.17 \cdot 10^{-9}$
I10	10	$1.82 \cdot 10^{-8}$	$3.47 \cdot 10^{-9}$
I11	11	$2.32 \cdot 10^{-8}$	$4.90 \cdot 10^{-9}$

## 1.4 Modeling the Electrical Impedance of a Nanocomposite

Chapter four describes an equivalent electrical impedance circuit model for our NCs fabricated using functionalized, multi-walled CNTs dispersed in reactive ethylene terpolymer. A circuit model is of interest since such a model can account for lossy and nonideal NC characteristics, predict NC impedances at different CNT volume fractions  $\phi$  or aspect ratios, and aid in circuit analysis. However, a universal /suitable circuit model for NCs may be difficult to develop for high frequencies, as passive circuit

element parameters idealized as frequency independent can vary with frequency due to skin effect, eddy currents, polarization losses and other factors.

Three electrical circuit impedance models were considered in our study: a constant phase element model (CPE), a two dimensional circuit model consisting of randomly-positioned resistors and capacitors (2D RC), and an equivalent series resistor model (ESR). Each model is associated with an equation for the complex electrical impedance. Each model also can be described with a resistor – capacitor passive element circuit model as shown in chapter four.

The CPE model has a constant electrical impedance phase angle =  $\arctan \left( \frac{\textit{imaginary impedance}}{\textit{real impedance}} \right)$  over a wide range of frequencies. Jonscher's universal power law for the complex permittivity also shows a constant phase angle behavior for the complex electrical susceptibility. CPE was selected due to the constant phase angle. CPE has two possible electrical impedance equations and either can be used at high frequency. The two alternate expressions for a CPE impedance arise from difficulties in understanding a physical interpretation for CPE.[12]

The ESR model consists of a frequency dependent resistor, a frequency independent resistor in parallel with an ideal capacitor; and an equivalent series inductor. The frequency dependent resistor is in series with the capacitor to represent frequency dependent resistances due to skin effect at the electrode leads or capacitor pads. This resistor also represents energy losses transformed as heat within the dielectric NC. The frequency independent resistor in parallel with the capacitor

represents a DC or low frequency percolation path(s) caused by the CNTs forming a network from the high side electrode to the low side electrode. This path is highly resistive compared to the capacitively coupled reactance and can be ignored in the model. The series inductance represents lead inductance from the measuring instrument's electrodes. Measuring equipment inductance is "tared out" during the compensation (calibration) procedure and is disregarded in our modeling.

The 2D RC model is a mixture of resistors and capacitors placed randomly and connected together within a square network. It has been determined that the total number of passive elements can be changed from 170, 512, or 2024 RC components without any significant change in the AC response.[13] We showed in chapter four that the proportion of resistors in the 2D RC circuit model is related to the loss tangent which was measured during our experiments. It was found that such a network gives the same electrical impedance characteristics as a three dimensional cubic network of resistors and capacitors.[14] This model was selected because a three dimensional circuit cubic network simulates a random mixture of microcapacitors and resistors. Such a system can describe an NC's internal mesoscopic geometry, where adjacent CNTs separated by a polymer dielectric form microcapacitors that couple capacitively; and dielectric losses and conducting CNTs represent resistors. An equation relating the loss tangent to the number of resistors in the 2D RC model is presented in chapter four.

The real and imaginary relative permittivities ( $\epsilon_r'$  and  $\epsilon_r''$  respectively) were measured for two average aspect ratio multi-walled CNTs (32 and 344) at varying

CNT volume fractions. The permittivities were measured from 80 MHz to 500 MHz using an Agilent E4991A material analyzer. The NC sample contacts upper and lower (parallel) electrodes on a model 16453A test fixture that attaches in a parallel plate arrangement to the material analyzer.

The real and imaginary electrical impedances ( $Z'$  and  $Z''$  respectively) for each NC sample were calculated using the relative permittivity measurements, where  $Z' = \frac{\epsilon_r''}{\omega C_o (\epsilon_r'^2 + \epsilon_r''^2)}$ , and  $Z'' = \frac{-\epsilon_r'}{\omega C_o (\epsilon_r'^2 + \epsilon_r''^2)}$ . These equations follow from the definition of the complex capacitance.

$Z'$  and  $Z''$  were fit to the aforementioned impedance model equations using OriginLab's data analysis software application. Goodness of fit was gauged using the squared correlation coefficient. The correlation coefficient indicates whether the data fits the impedance model without indicating which model is preferred. The 2D RC model has two fit parameters whereas the other models have one fit parameter. The empirical data is more likely to fit the 2D RC model since it has the greatest number of fit parameters. But the model with the most fit parameters may not be the most accurate representation of the physical problem under study. It is important to identify the best model since that model may provide insight into the NC's electrical characteristics and internal mesoscopic geometry. We used the Akaike Information Criterion numbers (AIC) to determine which model is preferred. AIC uses a statistical analysis to gauge the distance between the experimental impedance data and the impedance models under consideration. The model with the lowest AIC number has the shortest distance to the distribution representing the experimental data and so is the

preferred model. AIC does not indicate whether the experimental impedance data fits the preferred model. The correlation coefficient is used to determine whether the preferred model actually fits the experimental impedance data.

The CPE model was the preferred electrical impedance model for our NCs. The CPE and the 2D RC models had high squared correlation coefficient ( $> 0.999$ ) that exceeded that for the ESR model. This correlation coefficient is sufficiently large to show that all three models fit the experimental data. CPE had the lowest AIC number of the three models because CPE only requires one fit parameter whereas 2D RC requires two fit parameters. CPE was the preferred electrical impedance model for our NCs.

## **Chapter 2. Analysis of electrical percolation thresholds in carbon nanotube networks, using the Weibull probability distribution**

### **2.1 Introduction**

It is of scientific and technological interest to analyze the minimal concentration of carbon nanotubes (CNTs) necessary to form a percolating network. From a practical perspective, CNT networks have been proposed as constituents of thin film transistors[15] for electronics and biosensors[16], polymer composites for electromagnetic interference shielding[17], etc., While variability in device characteristics was considered[18], the widespread unpredictability in the intrinsic geometry, *e.g.*, the length ( $L$ ) of the CNTs, has not yet been modeled. Such issues with predictability of the geometry are typical of nanostructure synthesis processes and could strongly influence the electrical characteristics and device properties. The prediction of a threshold is also pertinent in the synthesis of CNT based composites, where the cost of the nanostructures is a major factor.

### **2.2 The Stochastic Percolation Model**

In this paper, we first use an excluded volume percolation theory based

model[19], [20] to estimate the theoretical critical volume percolation threshold,  $\phi_c$  of the CNTs, as a function of  $L$ . For this, we assume that the  $i^{th}$  CNT has a volume,  $v_i$ , in a polymer/insulating matrix of unit volume. Now, if the percolation threshold corresponds to the connectivity of  $N_c$  CNTs, then the odds of *not* selecting any CNT (corresponding to a point in the matrix) would be:

$$(1 - \phi_c) = (1 - v_1) \left( \frac{1 - v_1 - v_2}{1 - v_1} \right) \left( \frac{1 - v_1 - v_2 - v_3}{1 - v_1 - v_2} \right) \dots \left( \frac{1 - v_1 - v_2 - \dots - v_{N_c}}{1 - v_1 - v_2 - \dots - v_{N_c-1}} \right) = 1 - N_c \sum_{i=1}^{N_c} \frac{v_i}{N_c},$$

implying that

$$\phi_c = N_c E[v] \quad (1)$$

$E[v]$  denotes the expected value or ensemble average of the CNT volume. It is to be noted that equation (1) is distinct compared to the critical percolation threshold extant in literature, which assumes that the percolating objects are penetrable, *i.e.*, hitherto applied to pores in rock *etc.* In deriving equation (1), we have assumed that the CNTs were impenetrable. We then use the identity,  $E[v] = \frac{E[V_{ex}] N_c}{E[V_{ex}]}$  ( $\frac{E[v]}{N_c}$ ), where  $V_{ex}$  is

defined as the excluded volume[21]: the space circumscribed around the CNT by the center of another CNT, whereby both CNTs contact each other but do not overlap. For isotropically oriented, spherically capped *stick like* objects of diameter “ $D$ ” and random length “ $L$ ”, which we take to be akin to CNTs,

$E[V_{ex}] = \frac{4\pi}{3} D^3 + 2\pi D^2 E[L] + \frac{\pi}{2} D E[L^2]$ . Also, for the CNT modeled as a capped

cylinder,  $E[v] = \frac{\pi}{6} D^3 + \frac{\pi}{4} D^2 E[L]$ . Note that the CNT diameter is assumed to be

constant. For infinitely thin cylinders of deterministic length, Monte-Carlo simulations were used<sup>6</sup> to estimate  $E[V_{ex}]N_c$  as  $\sim 1.4$ . This is an upper bound when the lengths vary randomly, as  $E[V_{ex}]$  should be weighted to favor the longer CNTs. For a given  $D$ , the theoretical  $\phi_c$  would be:

$$\phi_c(L) = \frac{E[V_{ex}]N_c}{\frac{4\pi}{3}D^3 + 2\pi D^2 E[L] + \frac{\pi}{2}DE[L^2]} \left( \frac{\pi}{6}D^3 + \frac{\pi}{4}D^2 E[L] \right) \quad (2)$$

For a deterministic  $L$ , the variation of  $\phi_c$  as a function of the aspect ratio ( $= L/D$ ) is shown in Figure 2-1. Such a depiction necessarily implies that a definitive  $\phi_c$  is obtained at a given  $L$ . However, it is commonly observed both in our experiments<sup>3</sup> and in other examples from literature[22] that  $L$  is not a deterministic constant but should properly be considered a random variable, *i.e.*, as  $\underline{L}$ , that could have considerable variation. For example, we have measured subsequent to ultrasonication – a procedure necessary<sup>3</sup> for dispersion of the CNTs into polymer matrices, that single walled CNTs (SWCNTs) have lengths ranging from 2.2 – 7.8  $\mu\text{m}$  while multiwalled carbon nanotubes (MWCNTs) vary in length from 3.0 – 8.4  $\mu\text{m}$ . In another instance[23], a batch of SWCNTs synthesized through arc-based methods had  $L$  in the 0.7 – 4.3  $\mu\text{m}$  range. Such large variability clearly makes  $\phi_c$  a function of  $\underline{L}$  and would lead to uncertainties in obtaining an accurate percolation threshold.

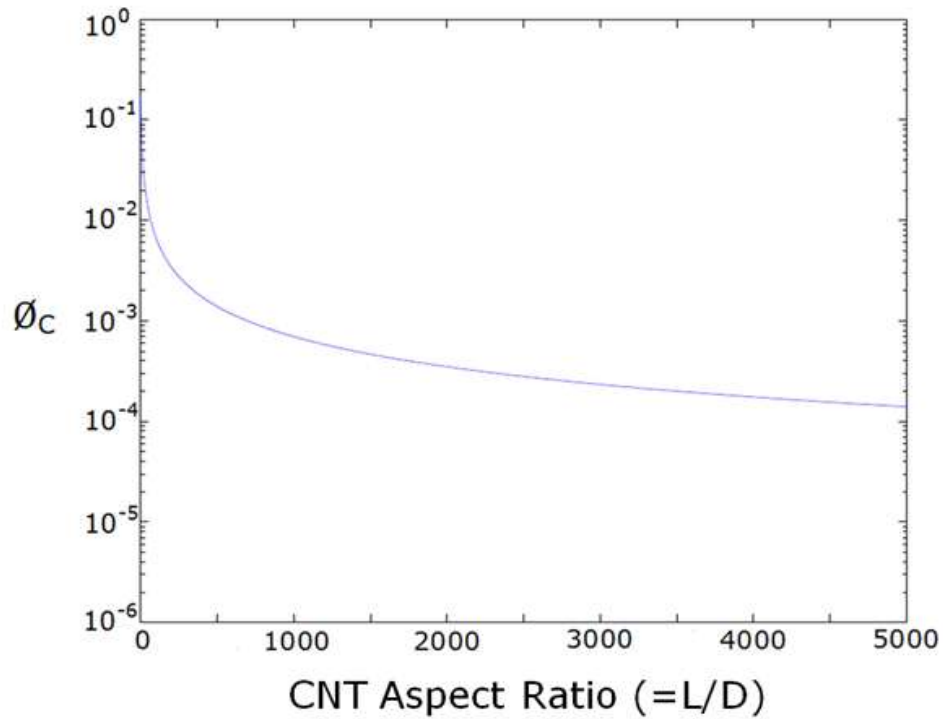


**Figure 2-1** The theoretical variation of the critical percolation threshold ( $\phi_c$ ) plotted as a function of the CNT aspect ratio ( $= L/D$ ) assuming a deterministic length and diameter.

The above issues also imply that a suitable stochastic model is necessary to evaluate the  $\phi_c$ , e.g., for a CNT/polymer composite[24] or a CNT network transistor[25], as  $\phi_c(\underline{L})$  is not equal to the  $\phi_c$  evaluated at the average CNT ensemble length, i.e.,  $\phi_c(E[\underline{L}])$ . A proper expression for  $\phi_c$  would account for variations in  $\underline{L}$  and could be expressed through the correlation, i.e.,  $E[\underline{L}^2]$ . The stochastic approach would then provide a theoretical value, i.e., a  $\phi_c(\underline{L})$  that accounts for the mean and

variance of  $\underline{L}$ . A theoretical value for  $\phi_c$  can be found from equation (2) where the average CNT length is now  $E[\underline{L}]$  with a variance,  $VAR[\underline{L}] = E[(\underline{L} - E[\underline{L}])^2] = E[\underline{L}^2] - (E[\underline{L}])^2$ . Both  $E[\underline{L}]$  and  $E[\underline{L}^2]$  can be evaluated by fitting empirical CNT length data to a probability density (p.d.f.). As the p.d.f. cannot be *a priori* determined, we use the sample mean length  $\mu_L$  and sample variance  $s_L^2$  as unbiased estimates of the population mean and variance[26].

## 2.3 Experimental

For the practical application of the above principles and experimental verification, we first dispersed carboxyl (-COOH) group functionalized SWCNTs and MWCNTs into a polymer. A reactive ethylene terpolymer (RET: Elvaloy 4170) constituted of an epoxide functional group was chosen for a polymer/insulating matrix, with the underlying rationale that the epoxide ring rupture[27] on the RET would be facilitated by the -COOH groups on the functionalized CNTs. The bonding between the -COOH and the epoxide group could help in the uniform dispersion. The exact location of the functional groups would depend on the defect density on the CNTs and can be manipulated[28]. However, if the defects are considered to be randomly dispersed, isotropic bonding of the CNTs with the polymer matrix is implied and yields uniform mixing. More details regarding the fabrication procedure and characterization of the composites have been reported elsewhere [29], [30].

The lengths of the CNTs in several composite samples were first measured

using a scanning electron microscope (SEM: Phillips XL30). In the case of SWCNTs, while the bundle diameters ( $D$ ) were noted to be  $\sim 4.8$  nm using atomic force microscopy (AFM), the length variation did not fit Gaussian, exponential, Rayleigh, log-normal, or Weibull - Figure 2-2 (a), distributions. The poor fit is attributed to a mixture of different probability densities of the SWCNT lengths within the composite. We then used our mean sample SWCNT length ( $\mu_L \sim 4.28$   $\mu\text{m}$ ) as an estimate of  $E[\underline{L}]$  and the sample variance of  $s_L^2 \sim 1.364$   $\mu\text{m}^2$  for estimating  $E[\underline{L}^2]$  ( $= \text{VAR}[\underline{L}] + E[\underline{L}]^2 \sim s_L^2 + \mu_L^2$ ). Using the upper bound of  $N_c E[V_{ex}]$ ,  $\sim 1.4$ , and substituting sample statistics,  $\mu_L$  and  $s_L^2$  in equation (1) yields a theoretical percolation threshold of  $\phi_c(\underline{L}) = 0.00073$ .

On the other hand, for the case of MWCNT bundles (with  $D \sim 188$  nm) the lengths were fit very satisfactorily to a Weibull distribution - Figure 2-2(b). For example, the value of the correlation coefficient for the MWCNT lengths,  $r^2$  ( $= 0.9833$ ), exceeds the tenth percentile of  $r^2$  ( $= 0.85$ ) established from Monte Carlo simulations using random numbers known to fit a Weibull distribution[31]. We also considered published literature from other groups on MWCNT length data[32], where again a satisfactory fit to a Weibull distribution was obtained - Figure 2-2(c).

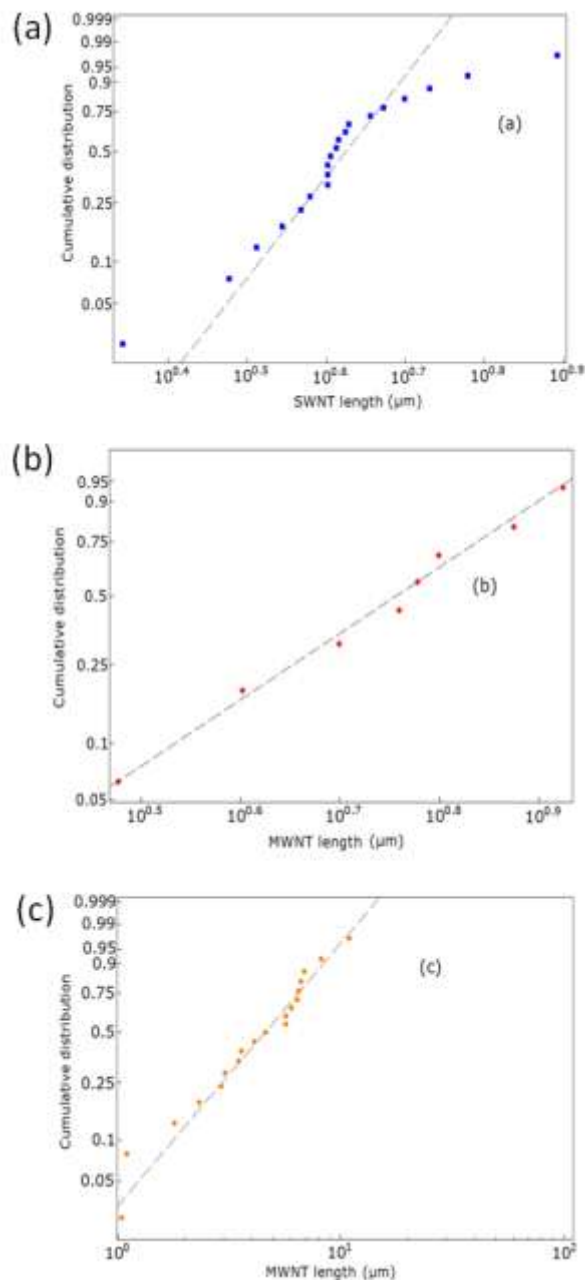


**Figure 2-2** The lengths of (a) SWCNTs, and (b) MWCNTs dispersed into the polymer matrix in the present study, and (c) MWCNTs from another study in literature [33] (Yu et al, Science, 287, 637 – 640, 2000), plotted on Weibull probability paper. Nonlinearities in (a) indicate a poor fit to a Weibull probability density while excellent fits were obtained for (b) and (c).

Generally, the  $n^{\text{th}}$  moment for a Weibull distribution is given by  $E[L^n]$ , where

$$E[L^n] = \theta^n \Gamma\left(\frac{n}{\beta} + 1\right) \quad (3)$$

$\Gamma$  denotes the Gamma function. A two parameter Weibull p.d.f. is then completely described by a shape parameter,  $\beta$  and the scale parameter  $\theta$ . For Figure 2-2(b),  $\beta = 3.97$  and  $\theta = 6.3525$  were calculated from the slope and intercept and were then used to find the statistical moments, *e.g.*, mean, correlation, skewness, kurtosis *etc.*, of the Weibull distribution[34]. To interpret these numbers, it is noted that for  $\beta = 3.6$ , the distribution of lengths would be symmetrical about the mean. A  $\beta > 3.6$  implies a left-hand skewness of the MWCNT length probability density, *i.e.*, more CNTs are shorter rather than longer, while a  $\beta < 3.6$  suggests the MWCNT lengths have a right-hand skewed distribution. Furthermore,  $\theta$  denotes the value below which ~63% of the NT lengths are smaller, *i.e.*, ~63% of the CNT lengths are less than 6.3525  $\mu\text{m}$ . Additionally, a high  $r^2$  on a Weibull plot suggests that the length distributions arise from a single probability density instead of a mixture of different probability densities. An  $r^2$  of ~ 0.9833, in Figure 2-2(b), then suggests that a single, particular mechanism could determine the length distribution, *e.g.*, a uniform mode of fracture at particular defects, due to the CNT processing. A poor fit, as with the SWCNT lengths in Figure 2-2(a), would indicate that the length distribution arises from a mixture of two or more distributions where each distribution is the outcome or consequence of a different event, *e.g.*, CNT fracture could occur at both defect-prone and defect-free sites, or could be mediated through multiple varieties of defects.

From the calculation of the moments, we determined for the case of Figure 2-

2(b) with MWCNTs, that  $\mu_L = 5.756 \text{ } \mu\text{m}$  and  $s_L^2 = 2.643 \text{ } \mu\text{m}^2$ . The substitution of these  $\mu_L$  and  $s_L^2$  values into equation (2) then yields a theoretical  $\phi_c(L) = 0.0193$ .

To experimentally analyze and correlate the influence of statistical variation on electrical percolation thresholds, we measured the electrical conductivity;  $\sigma$ . A four-point probe was used to measure the electrical resistance,  $R$ , for composites with  $R < 1 \text{ G}\Omega$ , using the Keithley 487 picoammeter and the Keithley 2400 Sourcemeter. For higher resistance ( $> 1 \text{ G}\Omega$ ) composites, two point measurements using the Agilent B1500A semiconductor device analyzer with triaxial probes were employed. For these measurements, samples with sputtered gold contacts were used. The experimental  $\phi_c$  for electrical percolation was then determined by fitting the measured  $\sigma$  of the CNT dispersed composites to the conductivity power law equation[35],  $\sigma = \sigma_0 (\phi - \phi_c)^t$ . Subsequently, for the SWCNT samples – Figure 2-3(a), we obtained from the fit to the  $\sigma$  variation, a  $\phi_c$  of 0.0011 which is quite close to the theoretical mean ( $\sim 0.00073$ ). In the case of MWCNT dispersed polymers, the  $\phi_c$  was found to be 0.0147 which, is again close to the theoretical mean of  $\sim 0.0193$ , predicted from stochastic theory.

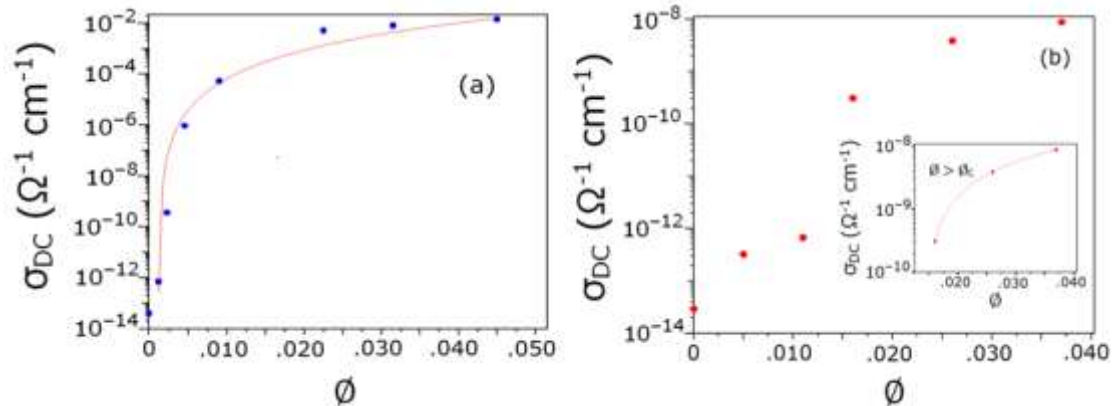


**Figure 2-3** The variation of the DC electrical conductivity ( $\sigma_{DC}$ ) with volume fraction ( $\phi$ ) for **(a)** SWCNTs and **(b)** MWCNTs dispersed in a polymer matrix, was used to determine the percolation threshold ( $\phi_c$ ). The inset in (b) indicates the fit of  $\sigma_{DC}$  to an expression of the form  $\sigma_{DC} \sim \sigma_0 (\phi - \phi_c)^t$  for  $\phi > \phi_c$ .

## 2.4 Conclusion

We conclude by positing that statistical analysis using a stochastic approach can be used to describe the impact of random CNT lengths on the electrical percolation thresholds. Such modeling could be used to *a priori* determine the thresholds while accounting for realistic process variability. The proposed methodology can be extended to other mutable CNT characteristics such as diameter, agglomeration, curvature, *etc.*

Chapter 2, in full, has been published in the *Journal of Applied Physics*, **108** 024305 (2010) “Analysis of electrical percolation thresholds in carbon nanotube networks using the Weibull probability distribution” by S. Pfeifer, S. H. Park, and P. R. Bandaru.

This paper was selected for republication in the *Virtual Journal of Nanoscale Science & Technology*, (July, 2010).

## **Chapter 3. A method for quantitatively characterizing the dispersion of nanostructures in polymers**

### **3.1 Introduction**

It is often necessary to quantitatively measure the degree of dispersion of microscopic and nanoscopic entities in a macroscopic polymer matrix. As an example for illustrating the applicability of such a notion, composites constituted of carbon nanotubes (CNTs) placed in a polymer[36][37] have been widely proposed for electromagnetic interference (EMI) shielding[38][39][40], in high sensitivity infrared sensors[41], structural applications[42],[43] *etc.* It has been generally accepted that the composite properties would be optimal when the CNTs are uniformly dispersed within the polymer matrix[44]. The uniform dispersal and bonding of CNTs in a polymer may confer unique properties to the composite, *e.g.*, through the postulated, formation of an *interphase* region[45], enhanced charge carrier scattering[46], *etc.* Similar considerations also apply to the dispersion of other structures such as nanoparticles[47], *e.g.*, used in polymer composite foams[48] where aggregation and bundling can lead to poor interfacial bonding of the structures with the polymer matrix. Bundling is not unexpected due to the strong van der Waals bonding prevalent in such structures. This in turn can cause variable and diminished properties in the composite. While single walled CNT (SWNT) and multi-walled CNT (MWNT) based composites have been reported[49] [50] [51] to have enhanced

elastic modulus and ultimate tensile strength, it has been frequently seen that beyond a certain loading fillers can be deleterious (*e.g.*  $\sim 0.6$  vol % in phenol/SWCNT composites[52] or polypropylene/SWCNT composites[53]), presumably due to bundling of the CNTs. In our own studies, we have seen a decrease in the work of fracture of a SWNT-RET (reactive ethylene terpolymer) composite at  $\sim 0.1$  vol % loading fraction of the nanotubes.[54]

It was also proposed that the nanostructure surfaces and interfaces could be functionalized through the use of suitable coupling agents[55], [56] and made to interact more homogeneously with the polymer matrix. However, it is practically difficult to uniformly disperse nanostructures as the very same characteristics that confer their unique properties (*e.g.*, high specific surface area) also encourage mutual attraction. It has also been shown[57] that commonly used homogenization techniques such as ultrasonification/blending could destructively reduce CNT length to diameter aspect ratio. While maintaining uniformity in dispersion is difficult and is presently an active research topic, it would nevertheless be pertinent to understand *quantitatively* or define more definitively the degree of dispersion of nanostructures, such as CNTs, within a polymer. This paper sets out to provide such a metric suitable for quantifying the dispersion allowing a comparison of the given distribution to a preferred distribution or pattern. We also suggest that our technique can be used for describing the dispersal of any minority phase within a majority phase.

### **3.2 Principles of the Approach**

A suitable dispersion metric should enable a comparison with either an idealized dispersion pattern or alternatively with a desired probability distribution (*e.g.*, uniform, Poisson distribution, *etc.*). From a more quantitative perspective, one example of a well-defined metric involves the use of the *quadrat* approach[58][59], valid at relatively low filler density in a matrix. In such a method, for example, the CNTs are located from a visual micrograph – obtained, *e.g.*, through transmission/scanning electron microscopy (TEM / SEM) based images of a composite cross-section. The image is then subdivided into several squares/*quadrats* and the number of pixels corresponding to the CNTs within each quadrat counted. A perfectly random/uniform arrangement of the dispersants within the matrix would then exhibit an equal number of centers in each quadrat, so that deviations may be gauged, *e.g.* by calculating the distance between distributions.

To this end, we first considered a random variable “ $\underline{X}$ ” that takes on discrete values,  $x_1, x_2, \dots, x_n$  with respective probabilities  $p_1, p_2, \dots, p_n$  given by some probability mass function,  $p_i$ . A measure of the randomness of the distribution is then  $-\log_2(p_i)$ , and the average randomness of  $\underline{X}$ , could be defined through:

$$H(\underline{X}) = -\sum_{i=1}^n p_i \log_2(p_i) \quad (1)$$

$H(\underline{X})$  can be used as the basis for quantifying the error (/distance) associated with comparing a given distribution “ $Q$ ” to a different distribution “ $P$ ”. Let “ $P$ ” and “ $Q$ ” have probability mass functions  $p_i$  and  $q_i$  respectively. From equation (1), the *distance* between these two distributions,  $D(P//Q)$ , is given by[60]:

$$\begin{aligned}
D(P//Q) &= - \left[ - \sum_{i=1}^n p_i \log_2(p_i) \right] - \sum_{i=1}^n p_i \log_2(q_i) \\
&= \sum_{i=1}^n p_i \log_2\left(\frac{p_i}{q_i}\right) \geq 0
\end{aligned} \tag{2}$$

This interpretation of the *distance* is then illustrated with respect to how a particular nanostructure distribution, say corresponding to “*Q*”, differs from a preferred / standard distribution corresponding to “*P*”, *e.g.* a Poisson or uniform (square, hexagonal lattice, *etc.*) distribution[61][62]. A corollary of the previous statement is that when a particular distribution “*Q*” approaches the preferred distribution “*P*”, the distance should approach zero. Generally,  $D(P//Q)$  is not a true distance metric since the equality  $D(P//Q) = D(Q//P)$  usually does not hold[63]. We postulate using  $d(P//Q)$  as follows[64]:

$$d(P//Q) \equiv \frac{1}{2} [D(P//Q) + D(Q//P)] \geq 0 \tag{3}$$

It is apparent that now,  $d(P//Q) = d(Q//P)$  and when the distributions are equivalent, *i.e.*,  $d(Q//Q) = 0$ .

### **3.3 Implementation of the $\langle d(P//Q) \rangle$ metric to gauge the uniformity of a given CNT distribution within a polymer matrix**

We will next outline the methodology for utilizing the above principles in quantifying the deviation of a given CNT distribution in a polymer from a standard distribution. Initially, an algorithm (implemented in MATLAB<sup>TM</sup>) was used to

generate 10,000 randomly positioned quadrats, imposed on a micrograph. Although the algorithm could have simply placed a quadrat centered at each pixel within the image, the use of such a random sample of quadrats saves computational time when evaluating larger micrographs, while providing a satisfactory representation of each image. Also, this allows the direct comparison between differently sized micrographs since the conventional approach of using a fixed quadrat grid would require a different number of quadrats for differently sized micrographs. Additionally, a fixed quadrat grid can result in significantly different dispersion metrics depending on where the grid is superimposed over the micrograph[65]. We also note that a sufficiently large quadrat square should be chosen to adequately characterize the actual CNT distribution, *e.g.*, if no CNT lies within a quadrat, the quadrat size should be increased until the expanded quadrat contains at least one pixel from a CNT. This is essential for equations (2) and (3) to be well-defined, as both  $p_i$  and  $q_i$  appear in the denominator and thus must be nonzero in each and every quadrat. Care was then taken to have an optimal quadrat size: larger quadrats can make a clustered distribution look uniform since they tend to have nearly the same number of CNTs, while smaller quadrats may not contain any CNTs.

Our program was then configured to yield the area fraction of the CNTs within each of the 10,000 quadrats. The CNT distribution probabilities,  $p_i$  - related to probability of finding CNTs within the  $i^{th}$  quadrat, were found through using the area  $a_i$  (in units of pixels) of the CNTs within the  $i^{th}$  quadrat of area  $A_i$ , through:

$$p_i = \frac{a_i / A_i}{\sum_{i=1}^n a_i / A_i} \quad (4)$$

The denominator normalizes the probability over the total number ( $n$ ) of quadrats, so that  $\sum_{i=1}^n p_i = 1$ . Equation (4) can also be used as an estimator of a probability function for deterministic patterns, *e.g.*, (i)  $p_i = 1/n$ , for a uniform distribution. However, of the five types of two-dimensional Bravais lattices, the hexagonal lattice could be considered the most well-dispersed since it has the largest number of equidistant nearest neighbors[66]. Consequently, for the purpose of a preferred/standard distribution a hexagonal lattice (HEX) was chosen. It is to be emphasized that our proposed approach and algorithm can be applied to any distribution, and we chose the HEX distribution only for illustrative purpose. It may also be desirable to change the density of the chosen/preferred pattern to represent a higher or lower volume fraction of the nanostructure dispersion. In this way, images of nanostructures dispersed in polymers can be compared to a preferred point pattern/lattice, using equation (4) as an estimator of the probability function. The  $a_i$  may also be considered a reasonable estimator of the CNT volume fraction.

For calculating the  $a_i$ , we had to consider carefully from digital images/micrographs the pixels that do represent CNTs. Generally, digital images are created by a quantization and sampling process which mathematically represents an image through a matrix of real numbers. Each matrix element corresponds to a pixel which is the smallest element of the image and is identified by its position within the image and a numerical value representing the degree of darkness of that pixel[67]. In

our processed images, the numerical value (with 8 bit resolution) could range from 0 (black) to 255 (white). We measured CNT and polymer pixel values within our micrographs using the ImageJ application (<http://rsbweb.nih.gov/ij/>) and determined, for our case (see Figure 3-1) that a 150 pixel value threshold could distinguish CNTs from the contrasting polymer background. Both MATLAB<sup>TM</sup> and ImageJ recognize pixels by their numerical value, and it is to be expected that other images corresponding to those produced by different equipment/imaging conditions may require a different threshold. The initial length of each quadrat square was then set to be 45 pixels which is approximately 3.5 times the average CNT diameter at 1250 X magnification (the exact conversion between pixels and CNT diameter would vary with the magnification[68]). Ten measurements of  $d (P//Q)$ , with respect to the HEX pattern, were averaged for any particular image / pattern under test to estimate the population average and lower the standard error estimate (as indicated in Table 3-1).

We then applied the above methodology to test the proposed dispersion metric, to both our own pattern images of CNTs dispersed in an epoxy polymer (reactive ethylene terpolymer: RET) as well as those published in literature[69][70]. The RET (Elvaloy 4170) was constituted of (1) polyethylene, (2) a polar methyl-methacrylate group, and (3) epoxide functional groups. While (1) and (2) contribute to mechanical elastomeric characteristics and corrosion resistance and are critical to the utility of RET as a hot-melt adhesive and coating, the epoxide group has high reactivity[71] and is amenable for effective anchoring of the constituent ring bonds with functional groups (*e.g.*, -OH, -COOH, -NH<sub>2</sub> etc.) on the CNTs[72], [73]. As the functional groups are associated with defects on the CNTs and are randomly dispersed, isotropic bonding

of the nanotubes with the polymer matrix was implied and expected to yield relatively uniform CNT dispersion. Both pristine and -COOH functionalized single walled CNTs (average diameter of 1.5 nm, length range ~ 5-20  $\mu\text{m}$ ), multi-walled CNTs (average diameter of 140 nm, length range ~ 5-9  $\mu\text{m}$ ), as well as coiled CNTs[74], [75] were used. Further details of the dispersal procedure and structural, electrical, and electromagnetic characterization have been reported previously[76], [77], [78].

Generally, considerable clumping reflective of CNT agglomeration was observed when unfunctionalized CNTs (to the left in Figure 3-1) were mixed into the polymer. We then observed that the general strategy of employing mutual chemical reaction between functional groups on the CNT and the polymer through covalent functionalization of the nanotube surface[79], [80] resulted in a relatively more uniform dispersion of SWCNTs in the polymer over a wide range of nanotube volume fractions, *i.e.*, from 0.2 vol % to 4.5 vol% (for functionalized coiled nanotubes and multi-walled nanotubes, in the center and to the right of Figure 3-1, respectively).

We now characterize the extent of uniformity in the CNT dispersed RET polymer through the  $\langle d(P//Q) \rangle$  metric, as applied to SEM images of the distribution of unfunctionalized and functionalized CNTs in the polymer (Figure 3-1). It is to be noted that the contrast between the CNTs and RET polymer matrix was enhanced using ImageJ prior to the implementation of the algorithm which enhances the sensitivity of CNT detection. Localized image areas may exhibit lower subject contrast between the CNTs and the polymer due to composite surface topology, electron backscatter at angular fracture surfaces, *etc.* The use of ImageJ visibly improved image contrast when the CNT and polymer pixel values were close to the 150 pixel

value threshold. Table 3-1 shows the  $\langle d(\text{Image} \parallel \text{HEX}) \rangle$  metric comparing each image in Figure 3-1 to a standard hexagonal pattern. Table 3-1 then shows the  $d$ -metric could be a quantitative measure of the extent of dispersion, yielding progressively larger values for images that exhibit greater clustering/poor dispersion and deviating more from the chosen hexagonal lattice standard. The numerical values are indicative of the number of bits representing the difference/distance between the given and the standard distribution[81].

We also compared the utility of the  $d(P//Q)$  metric with other results from literature (Figure 3-2 – taken from[82] and Figure 3-3 – taken from[83]). In the former case, the importance of reducing particle size to increase the degree of matrix/polymer reinforcement was discussed[84]. In the paper by Khare and Burris[85], a metric termed the free-space length,  $L_f$  correlates to the “characteristic size of the unreinforced polymer domains” and was defined as the “width of the largest randomly placed square for which the most probable number of intersecting particles is zero.” Figure 3-2, taken from this paper, shows nanoparticle dispersions categorized using such a method. This approach is equivalent to measuring the mean length of the largest quadrat square likely to contain zero particles, and has a potential drawback in that a large  $L_f$  could be indicated for low volume fraction CNTs and that it does not compare images to a desired pattern/distribution. Consequently, we analyzed the micrographs in Figure 3-2 using our  $d$ -metric approach, and the obtained results are indicated in Table 3-2. The comparison is now to a uniform distribution, with an implicit assumption that this is the desired distribution. The steadily increasing  $d$ -metric values from the top to the bottom, in the order (a) < (b) < (c) < (d), are in

accordance with the easily observed diminished uniformity of dispersion and now indicate a quantifiable measures of the degree of dispersion.

In yet another study taken from literature, the dispersion of alumina nanoparticles in a polyethylene terephthalate (PET) polymer matrix was investigated[86] through sample cross-sections taken from the composite (as given in Figure 3-3). The authors' analysis of the degree of dispersion was considered inadequate, as there was no obvious discrimination between single nanoparticles *vs.* an agglomeration of contiguous nanoparticles and in addition, no comparison was made to a standard/preferred pattern. We then applied our *d*-metric based approach to Figure 3-3, with the results indicated in Table 3-3. The comparison is again to a hexagonal pattern. The steadily increasing *d*-metric values from the top to the bottom, for both columns, now indicate definitive and well founded values for the degree of dispersion for published images.

Our methodology may also be adapted for three-dimensional images. Cross-sections of two-dimensional section scans at varying depths can be combined into a collage and our algorithm applied without modification. Alternatively, each cross-section can be evaluated individually and the *d*-metric dispersions evaluated at increasing cross-sectional depths. Such an evaluation can be easily accomplished, for example, by plotting the *d*-metric on statistical control charts[87]. The algorithm also can be adapted to three-dimensional imaging techniques through replacing quadrats with cuboids and area fractions with volume fractions.

### 3.4 Conclusion

We have shown conclusively that the  $d$ -metric, based on equation (3), can be used to satisfactorily describe nanostructure dispersion in polymer composites. The metric was applied to micrographs of CNT-polymer composites, taken from our own studies as well as nanoparticle-polymer composites from other studies in literature, and yields a measure of the degree of uniformity relative to a preferred/standard distribution. The proposed measure incorporates a firm mathematical basis and has the advantage that the deviation of a given distribution from a standard distribution can be quantitatively gauged.

Chapter 3, in full, has been submitted for publication in *Nanotechnology* “A method for quantitatively characterizing the dispersion of nanostructures in polymer composites” by S. Pfeifer and P. R. Bandaru.

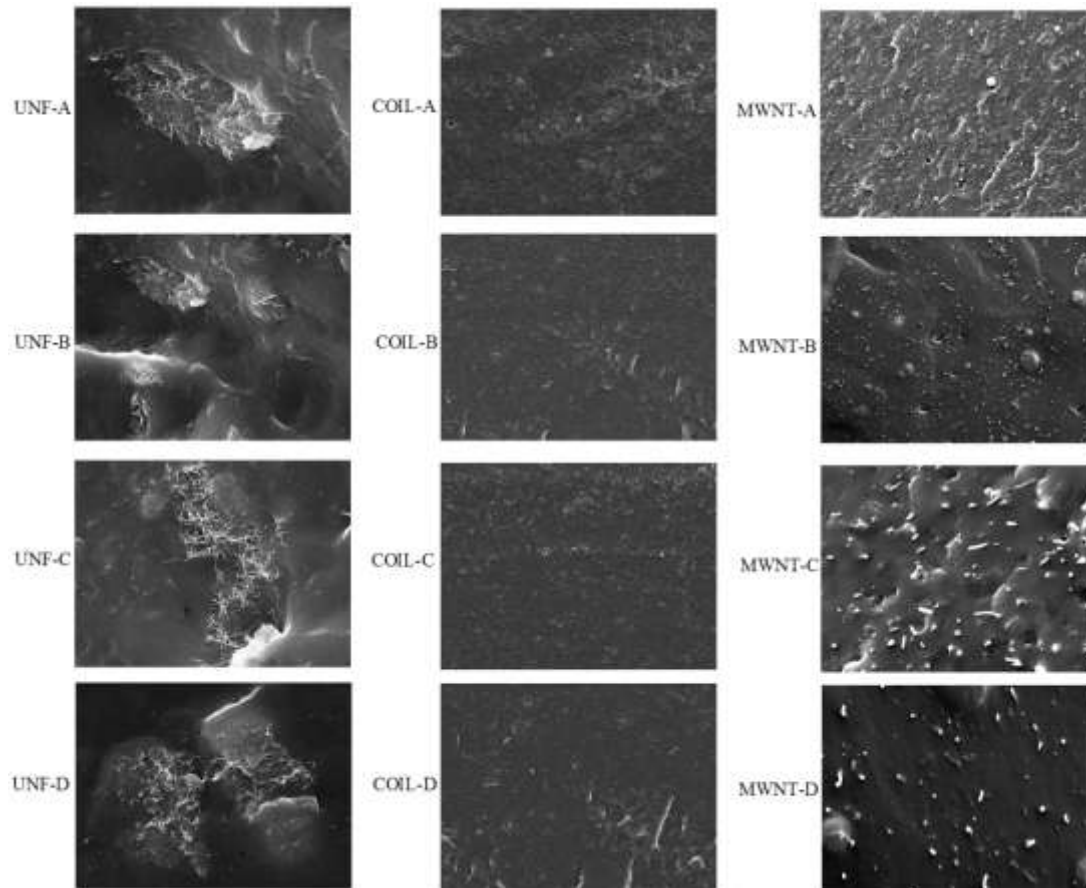


**Figure 3-1** The uniformity of dispersion of carbon nanotubes (CNTs) dispersed in a RET polymer matrix, decreases from the top to the bottom in these Scanning Electron Microscope (SEM) micrographs and a quantitative measure can be obtained through a *d*-metric analysis - Table 3-1. Left column: Increasingly poor dispersion of unfunctionalized CNTs (increasing from the top, UNF-A to the bottom, i.e., UNF-D). Center column: Increasingly poor dispersion of coiled CNTs (increasing from the top, COIL-A to the bottom, i.e., COIL-D). Right column: Increasingly poor dispersion of multi-walled CNTs, (increasing from the top, MWNT-A to the bottom, i.e., MWNT-D)

[Figure 3-2 was omitted from this dissertation but can be reviewed as figure 5 in the paper by Khare and Burris, *Polymer*, 51, 719, 2010]

**Figure 3-2** (Image taken from the paper by Khare and Burris, *Polymer*, 51, 719, 2010)

Our proposed  $d$ -metric can be used to analyze the dispersion of nanoparticles, as well and indicates steadily decreasing uniformity from (a) to (d) – Table 3-2.

[Figure 3-3 was omitted from this dissertation but can be reviewed as columns 2 and 4, figure 1 (A to D) in the paper by Kim, Lee, Barry and Mead, *Microscopy Research and Technique*, 70, 539, 2007]

**Figure 3-3** Another example of the application of the  $d$ -metric to the dispersion of alumina nanoparticles in PET polymer through the analysis of a TEM (transmission electron microscope) image from literature (Image taken from the paper by Kim, Lee, Barry and Mead, *Microscopy Research and Technique*, 70, 539, 2007). The non-uniformity of dispersion increases from A1 – D1 and A2 – D2. The dispersion metric results are presented in Table 3-3.

**Table 3-1** The  $d$ -metric for the images of Figure 3-1, indicate a quantification of the degree/uniformity of dispersion. While the numbers in **bold** indicate the  $d$ -metric values, the standard deviation from ten measurements is indicated in the brackets.

$\langle d(\text{HEX} \parallel \text{Pattern}) \rangle$	$\langle d(\text{HEX} \parallel \text{Pattern}) \rangle$	$\langle d(\text{HEX} \parallel \text{Pattern}) \rangle$
$\langle d(\text{HEX} \parallel \text{UNF-A}) \rangle =$ <b>5.805</b> (0.007)	$\langle d(\text{HEX} \parallel \text{COIL-A}) \rangle =$ <b>0.858</b> (0.004)	$\langle d(\text{HEX} \parallel \text{MWNT-A}) \rangle =$ <b>0.275</b> (0.001)
$\langle d(\text{HEX} \parallel \text{UNF-B}) \rangle =$ <b>5.815</b> (0.009)	$\langle d(\text{HEX} \parallel \text{COIL-B}) \rangle =$ <b>1.259</b> (0.011)	$\langle d(\text{HEX} \parallel \text{MWNT-B}) \rangle =$ <b>0.623</b> (0.004)
$\langle d(\text{HEX} \parallel \text{UNF-C}) \rangle =$ <b>6.092</b> (0.011)	$\langle d(\text{HEX} \parallel \text{COIL-C}) \rangle =$ <b>1.721</b> (0.015)	$\langle d(\text{HEX} \parallel \text{MWNT-C}) \rangle =$ <b>3.040</b> (0.002)
$\langle d(\text{HEX} \parallel \text{UNF-D}) \rangle =$ <b>6.577</b> (0.009)	$\langle d(\text{HEX} \parallel \text{COIL-D}) \rangle =$ <b>2.831</b> (0.007)	$\langle d(\text{HEX} \parallel \text{MWNT-D}) \rangle =$ <b>4.690</b> (0.007)

**Table 3-2** The  $d$ -metric for the images in Figure 3-2, indicate a quantification of the degree/uniformity of dispersion. While the numbers in **bold** indicate the  $d$ -metric values, the standard deviation from ten measurements is indicated in the brackets.

<b>&lt;d(Uniform    Pattern &gt;</b>
< $d$ (Uniform    a > = <b>0.021</b> (0.001)
< $d$ (Uniform    b > = <b>0.066</b> (0.001)
< $d$ (Uniform    c > = <b>0.153</b> (0.003)
< $d$ (Uniform    d > = <b>1.354</b> (0.007)

**Table 3-3** The  $d$ -metric for the images in Figure 3-3, indicate a quantification of the degree/uniformity of dispersion. While the numbers in **bold** indicate the  $d$ -metric values, the standard deviation from ten measurements is indicated in the brackets.

$\langle d(\text{HEX} \parallel \text{Pattern}) \rangle$	$\langle d(\text{HEX} \parallel \text{Pattern}) \rangle$
$\langle d(\text{HEX} \parallel \text{A-1}) \rangle = \mathbf{0.293}$ (0.002)	$\langle d(\text{HEX} \parallel \text{A-2}) \rangle = \mathbf{0.306}$ (0.001)
$\langle d(\text{HEX} \parallel \text{B-1}) \rangle = \mathbf{0.468}$ (0.002)	$\langle d(\text{HEX} \parallel \text{B-2}) \rangle = \mathbf{0.322}$ (0.001)
$\langle d(\text{HEX} \parallel \text{C-1}) \rangle = \mathbf{0.710}$ (0.005)	$\langle d(\text{HEX} \parallel \text{C-2}) \rangle = \mathbf{0.630}$ (0.002)
$\langle d(\text{HEX} \parallel \text{D-1}) \rangle = \mathbf{0.717}$ (0.002)	$\langle d(\text{HEX} \parallel \text{D-2}) \rangle = \mathbf{1.282}$ (0.004)

Chapter 3, in full, has been submitted for publication in *Nanotechnology* “A method for quantitatively characterizing the dispersion of nanostructures in polymer composites” by S. Pfeifer and P. R. Bandaru. Figure 3-2 was omitted from this dissertation but can be viewed as figure 5 in the paper by Khare and Burris, *Polymer*, 51, 719, 2010. Figure 3-3 was omitted from this dissertation but can be viewed as figure 1 in the paper by Kim, Lee, Barry and Mead, *Microscopy Research and Technique*, 70, 539, 2007.

# **Chapter 4. Modeling the relative dielectric permittivity and impedance of carbon nanotube constituted polymer composites**

## **4.1 Introduction**

The determination and modeling of the electromagnetic (EM) characteristics of carbon nanotube (CNT) containing polymer composites is of interest, with the objectives of obtaining (a) fundamental understanding of the influence of large aspect ratio electrical conductors, as well as for (b) practical applications. A large length to diameter aspect ratio, which could be as much as  $10^6$  (for a nanotube 1 mm length and 1 nm diameter) enables pertinent electrical characteristics to be obtained at much lower volume fractions, *e.g.*, at  $< 0.01\%$  nanotube filler concentrations[88]. In the context of applications, CNT containing composites have been advocated for a wide variety of uses, *e.g.*, EM interference shielding[89], thermal management[90], energy conversion[91], and electronic packaging applications[92], *etc.*, in which detailed characterization and understanding of the EM properties would be important.

In this paper, we report on the measurement, modeling, and interpretation of the relative dielectric permittivity ( $\epsilon_r^*$ ) of multi-walled CNT (MWCNT) – polymer composites at frequencies ( $f$ ) less than 500 MHz. The real and imaginary parts of  $\epsilon_r^*$  were then fit to real and imaginary electrical impedances and compared to lumped and distributed models of the resistance ( $R$ ) and capacitance ( $C$ ) of the nanotube – polymer

composite. At the very outset, a CNT – polymer composite was modeled to be of three constituents, *i.e.*, (1) an electrically conducting CNT (as is typical to MWCNTs) phase, (2) a relatively insulating polymer matrix, and additionally (3) an interphase[93] component. A relevant circuit model would then consist of equivalent electrical  $R$  and  $C$ . The inductive response of the measurement instrumentation and the composite sample was negligible (the relative magnetic permeability,  $\mu_r$ , of the sample was measured[94] to be  $\sim 1$ ), and could be subtracted out through calibration at the considered frequencies.

## 4.2 Experimental Procedure

We incorporated various filler fractions (in the range of 0 – 10 volume %) of acid-functionalized MWCNTs into reactive ethylene terpolymer (RET) based polymers through procedures that have been previously reported[95]. Samples of MWCNTs, with constituent diameters of  $\sim 20$  nm, and average length of  $\sim 6.8$   $\mu\text{m}$ , yielding an aspect ratio of  $\sim 340$ , were used. The geometrical parameters were determined, by scanning electron microscopy (SEM), through subjecting the MWCNTs to similar processing conditions as were used for their dispersion into the polymer. RET (Elvaloy 4170 from DuPont) constituted from (1) polyethylene, (2) a polar methyl-methacrylate, and (3) epoxide functional groups was seen to possess superior mechanical characteristics and corrosion resistance, while the epoxy group has high reactivity[96] and is amenable for effective anchoring of the epoxide ring bonds with functional groups (*e.g.*, -OH, COOH, -NH<sub>2</sub> etc.) on the CNTs, as was verified through Fourier transform infrared spectroscopy[97]. The uniformity of the

dispersion was gauged by considering scanning electron microscopy (SEM) micrographs at different length scales, *i.e.*, 1  $\mu\text{m}$  to 200  $\mu\text{m}$ , and the extensive use of image processing software and algorithms[98]. The permittivity was measured and modeled (over a frequency range of 80 MHz – 500 MHz, as used for line-of-sight communications[99]) using a RF Impedance/Material Analyzer (Agilent E4991A), with the composite sample contacting the upper and lower electrodes in the test fixture (Agilent 16453A). Prior instrumental calibration, using known Teflon® and silica glass standards, was used to validate the experimental setup. Additionally, the electrode and instrument inductances were compensated, through standard instrument testing protocols[100] with connected / open electrodes.

The complex permittivity,  $\varepsilon^*$ , is related to the real ( $\varepsilon_r'$ ) and imaginary ( $\varepsilon_r''$ ) components through  $\varepsilon^* = \varepsilon_0 (\varepsilon_r' - j\varepsilon_r'')$ , where  $\varepsilon_0$  is the permittivity of free space ( $=8.854 \cdot 10^{-12}$  F/m) and  $j = \sqrt{-1}$ . Representative experimental measurements are indicated in **Figure 4-1**. The electrical impedance,  $Z^* = Z' + jZ''$ , constituted of real ( $Z'$ ) and imaginary ( $Z''$ ) components was then calculated from the complex capacitance  $C_s^*(\omega)$  where  $\omega (=2\pi f)$ , is the angular frequency

$$\varepsilon_r^* (= \frac{C_s^*(\omega)}{C_o} = \frac{1}{j\omega Z^* C_o}), \text{ and } C_o = \frac{\varepsilon_o A}{L}, \text{ with } A \text{ as the electrode area and } L \text{ the}$$

distance between the electrodes. Consequently,  $Z' = \frac{\varepsilon_r''}{\omega C_o (\varepsilon_r'^2 + \varepsilon_r''^2)}$  and  $Z'' =$

$$\frac{-\varepsilon_r'}{\omega C_o (\varepsilon_r'^2 + \varepsilon_r''^2)}. \text{ Plots for the frequency dispersion of } Z' \text{ and } Z'' \text{ were calculated from}$$

$\varepsilon_r'$  and  $\varepsilon_r''$ , and have been indicated in **Figure 4-2**.

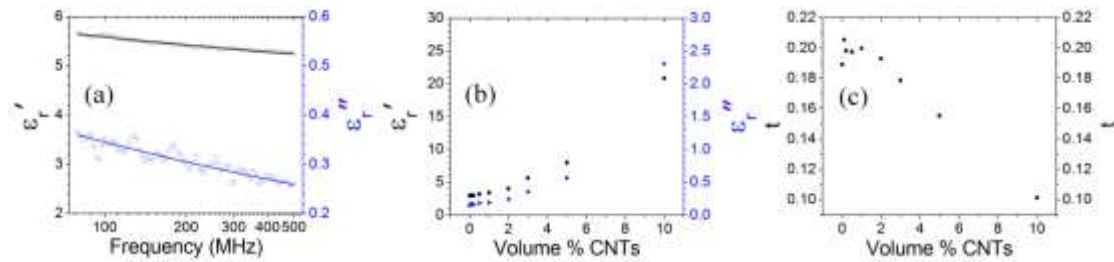


**Figure 4-1.** The variation of the real ( $\epsilon_r'$ ) and imaginary ( $\epsilon_r''$ ) dielectric permittivity with (a) frequency ( $\omega$ ) (with 3 vol % CNT fillers) and (b) CNT filler concentrations (at 100 MHz). In (a) the fit lines to the data (points) followed a power law relation, with  $\epsilon_r' (= a \omega^{-t} + b)$  and  $\epsilon_r'' (= d \omega^{-t})$  varying as  $\sim \omega^{-t}$  ( $a$ ,  $b$ ,  $d$ , and  $t$  are fitting parameters). (c) The variation of the power law exponent,  $t$ , with CNT filler concentration.

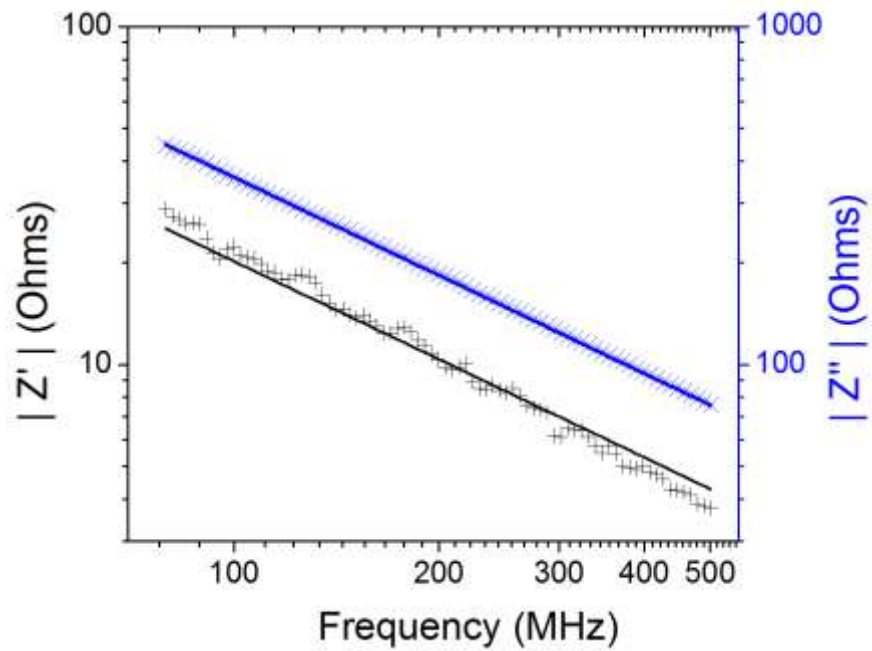


**Figure 4-2.** The variation of the real ( $Z'$ ) and imaginary ( $Z''$ ) parts of the electrical impedance ( $Z^*$ ) with frequency (with 3 vol % CNT fillers), as obtained from  $\epsilon_r'$  and  $\epsilon_r''$ .

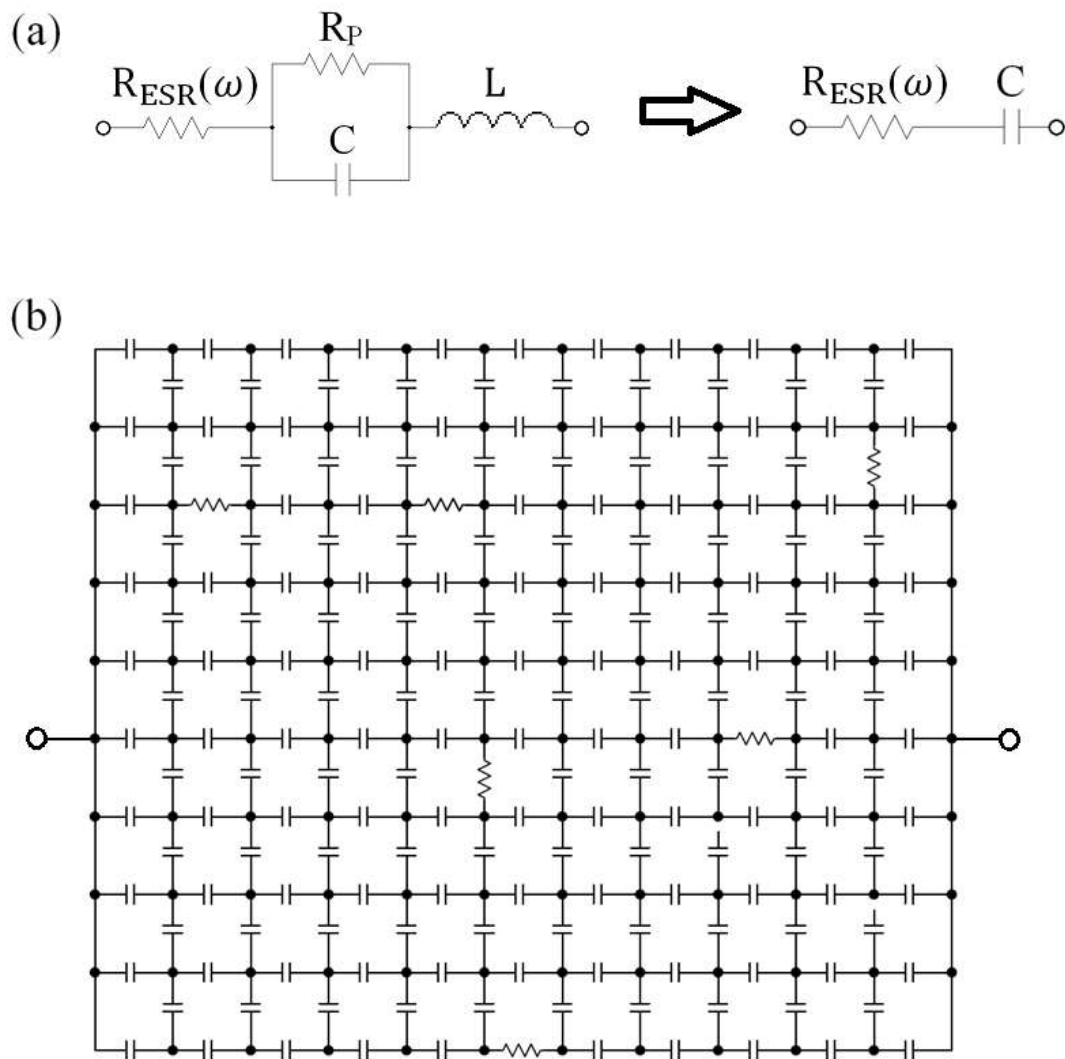


**Figure 4-3.** Circuit models for (a) an equivalent series resistance (ESR) model, and (b) a two-dimensional random network of resistors and capacitors (2D RC) model, were used to fit the  $Z^*$  variation (from Figure 4-2) of the nanotube-polymer composites.

### 4.3 Electrical Impedance Models

We compared electrical circuit models (see **Figure 4-3**) to characterize the  $Z^*$  (and  $\varepsilon_r^*$ ) variation in the nanotube – polymer composite, using using (i) an equivalent series resistance (ESR) model, (ii) a two-dimensional random network of resistors and capacitors (2D RC) model[101], and a derivative (iii) constant phase element (CPE) model[102]. The idea behind such various representations was to investigate whether the *net* impedance, in terms of the resistance and capacitance of the composite, could be considered in terms of lumped or distributed elements, and estimate the number of minimum needed fitting parameters. In the represented ESR model, of **Figure 4-3 (a)**,  $R_{ESR}(\omega)$  embodies the frequency dependent dielectric polarization losses and  $R_p$  accounts for the leakage currents in the capacitor. We could neglect  $R_p$ , compared to the capacitive impedance  $X_c (=1/\omega C)$  at volume fractions above the percolation threshold ( $\phi_c$ ), which was measured to be  $\sim 0.17$  vol% for composites using nanotubes of aspect ratio  $\sim 340$ . For example, at a CNT volume concentration of 2.6%, the  $R_p$  was estimated to be  $10^8$  times larger than the  $X_c$  at 1 GHz. Then,  $Z^* = R_{ESR}(\omega) - j/\omega C$

$$= [\tan(\delta) - j] / \omega C, \text{ where } \tan(\delta) = -\frac{Z'}{Z''} = \frac{\varepsilon_r''}{\varepsilon_r'}$$

the real and imaginary components of the impedance/dielectric permittivity.

The 2D RC model considers the composite with dispersed nanotubes and the intervening polymer to form a *distributed* electrical network of resistors and capacitors (e.g., constituted of the dielectric between the conductors/nanotubes). It has been previously shown that a three dimensional dispersion may adequately be represented through a two-dimensional network model[103]. The complex impedance was then

derived to be:  $Z^* = \frac{LR^{1-\beta}}{A(j\omega C)^\beta} = \frac{LR}{A(\omega RC)^\beta} \left[ \cos\left(\frac{\beta\pi}{2}\right) - j \sin\left(\frac{\beta\pi}{2}\right) \right]$ , and fitted to our experimental data. The 2D RC model is displayed, in **Figure 4-3(b)**, with 194 capacitors and 6 resistors corresponding to a  $\beta = 0.97$  ( $=194/200$ ), obtained through the fits.

While the ESR model considered a frequency dependent resistance, the CPE based representation invokes a distribution/dispersion of relaxation times,  $\tau(\omega)$ . While such models have been extensively used to parameterize the frequency response of solid electrolytes[104] and solid-solid interfaces[105], the present work is the first to utilize the CPE construct for the description of the electrical behavior of CNT – polymer composites. From a physical point of view, the influences of non-uniform potential and current distribution, roughness, composition variations, *etc.*, are some of the parameters[106] that could be described through such a model. The underlying idea of the CPE is to fit the impedance data, say that obtained through the distributed RC type model, over a defined frequency range. The constraint of a frequency range then implies that the electrical impedance,  $Z^* = \frac{1}{(Q\omega)^\beta} \left[ \cos\left(\frac{\beta\pi}{2}\right) - j \sin\left(\frac{\beta\pi}{2}\right) \right]$ , with  $Q$  as the only fitting parameter, and which can be reduced to resistive ( $\beta=0$ ), inductive ( $\beta=-1$ ), or capacitive ( $\beta=1$ ) behaviors. The CPE aspect is manifested through the  $\frac{Z''}{Z'}$  ratio, from which the magnitude of the phase  $\beta\pi/2$  is  $\omega$ -independent.

## 4.4 Discussion

As a result of the data fitting, detailed statistical analysis indicated that the coefficient of determination[107] (*i.e.*, the  $r^2$  value) was larger for the distributed models (2D RC and CPE) compared to the lumped (ESR based) model. Another important metric to describe the goodness of fit between competing models uses the Akaike Information Criterion (AIC)[108]. The underlying idea behind the AIC is that it incorporates a penalty for increasing the number of fitting parameters and consequently, a model with the minimum number of fitting parameters is preferred and given a low AIC number. We have then generally found a lower AIC number for the CPE and the 2D RC models, *e.g.*, for a 1 vol% (and 3 vol%) nanotube filler percentages, the AIC numbers were 239 (58) and 241 (60). The corresponding numbers for the ESR model were 523 and 379 respectively. We thus conclude that distributed models may more accurately determine nanotube – polymer composite properties.

From considering the  $\sigma^*$  ( $= j\omega\varepsilon_0 [\varepsilon_r' - j\varepsilon_r'']$ ) for the composite and the polymer and assuming that  $\sigma_N^*$  for the nanotube is purely real, we obtained a functional relation for the frequency dispersion of the composite dielectric constants, both for  $\varepsilon_r'$  as well as  $\varepsilon_r''$  to be varying as  $\omega^{p-t}$ . We have then fitted our experimental data – see **Figure 4-1(c)**, to the forms  $\varepsilon_r' = a \omega^{-t} + b$ , and  $\varepsilon_r'' = d \omega^{-t}$ , where  $a$ ,  $b$ ,  $d$ , and  $t$  are fitting parameters. It would then be expected that as the contribution from the polymer decreases (*i.e.*,  $p$  decreases) due to increasing the nanotube fillers, that  $t$  should increase. However, an opposite trend was observed as indicated in **Figure 4-**

**1(c).** We then hypothesize that the original assumption, *i.e.*, that  $\sigma_N^*$  is purely real, may not be correct and a complex conductivity, proportional to  $\omega$  should be considered. Consequently, the frequency dispersion of the composite for  $\varepsilon_r'$  as well as  $\varepsilon_r''$  would vary as  $\omega^{p+n-1}$ . If the decrease in  $p$  is lower than the increase in  $n$ , the correct trend in  $t$  could be obtained.

We justify the frequency dispersion of the nanotube fillers on the basis that its constituent electromagnetic properties could change depending on the environment, *e.g.*, the formation of an interphase[109] region could considerably modify the relative contributions of the filler and the polymer matrix. We have seen, for example, a smaller variation of the exponent,  $t$ , when lower aspect ratio nanotubes were used. It was also noted, from **Figure 4-1(c)**, that the  $t$  tends to  $(p-1)$ , as  $p$  decreases[110], which may indicate increasing contribution from the nanotubes. The  $t$  values were similar to those reported earlier[111] for multiwall MWCNT/poly-vinylidene fluoride (PVDF) composites. However, unlike this earlier study, we have not observed a drastic increase in the dielectric constants at the electrical conductivity percolation threshold ( $\phi_c$ ), due to the higher frequencies.

## 4.5 Conclusion

In summary, we have shown that the electromagnetic characteristics of nanotube-RET polymer composites could be best modeled by considering a constant phase element (CPE) based approach with frequency dependent resistances and capacitances.

Chapter 4, in full, has been submitted to the *Journal of Applied Physics* “A comparison of models for determining the relative permittivity of nanotube constituted polymer composites” by S. Pfeifer, S. H. Park, and P. R. Bandaru. (2012).

## Chapter 5. Summary of the Dissertation

Our research resolves three extant problems in nanocomposite research. First: we developed an equation that gives the critical volume fraction of CNTs required to achieve percolation when the CNT lengths vary randomly. This equation also establishes CNT percolation thresholds when the CNT lengths are deterministic. Second: our dispersion algorithm provides a single metric describing the degree of dispersion of any minority phase in a majority phase. This algorithm can be adapted to three dimensional, greyscale, or colorized images. The algorithm has sufficient versatility to compare an image to either another image or to a probability distribution. Third: a constant phase element electrical complex impedance model was described and validated experimentally for the nanocomposites under study.

In the electrical percolation threshold study, we have observed that electrical percolation can be achieved at very low CNT volume fractions (e.g.  $<10^{-3}$  critical volume fraction for  $\sim 1000$  CNT aspect ratio). Electrical percolation can be critical to achieving a conductive surface. Material applications include radar absorption or electro-magnetic shielding. The fabrication and processing of nanocomposites necessarily involves homogenizing operations that can alter and randomize the CNT lengths. The impact of random CNT lengths was successfully described by our percolation equation using a stochastic approach.

The nanometric sizes of the minority phase in nanocomposite research can yield novel materials properties. Concurrently the nanoscale size also brings a real

problem associated with achieving the correct level of dispersion to achieve those novel properties. It is difficult to disperse nanostructures as van der Waals forces tend to cause particle clustering and agglomeration. Homogenization techniques can damage the nanostructures and add time and cost to the fabrication process. Our dispersion algorithm provides an objective way to categorize the level of dispersion evident after nanocomposite fabrication.

The dispersion algorithm has considerable versatility. Three dimensional scans only require the substitution of cuboids (replacing quadrats) and inclusion volume fraction tallies (replacing inclusion area fraction counts). The algorithm also can be adapted to categorize greyscale or color images. In the nanocomposite study we used a pixel value threshold number to demarcate and distinguish the minority phase from the majority phase. For a greyscale or color image, this threshold would be replaced with bins. The bins would span a range of pixel values representing colors of interest. Pixel counts would be tallied for each bin and the *d-metric* used to compare the image to a desired, idealized pattern / image.

Our dispersion algorithm distinguished patterns from the literature that are considered to be severe tests of a dispersion metric. The underlying foundation for the *d-metric* is based on sound and proven principles of information theory. We also categorized SEM scans of cross-sections of our CNT / RET nanocomposite samples and successfully grouped these samples in order of dispersion.

The dispersion algorithm has the flexibility to compare an image to a desired probability distribution (i.e. uniform, Poisson, *etc.*) as well as to another image. The ideal image standard used for comparison can use different minority phase area

fractions to represent different desired volume fractions. (Stereologists have proven that particle area fractions measured from cross-sectional images are reliable estimators of volume fractions) [112].

In the study of high frequency complex permittivities and complex electrical impedances, we have described the fit of our nanocomposites to Jonscher's universal power law. The permittivities were used to calculate the complex electrical impedance from 80 MHz – 500 MHz. Three electrical circuit models were provided for three impedance equations (CPE, ESR, and 2D RC). While all three models fit the electrical impedance experimental data, the CPE model was shown to be the preferred model.

The permittivity research showed that a CPE model can be used to predict high frequency electrical behavior, including capacitive energy storage and dielectric losses. Ongoing research indicates that the exponent appearing in the equation for the CPE impedance could be related to the volume fraction dielectric at higher CNT volume fractions (Lichtenecker's permittivity mixing equation for an isotropic NC)[113]. Further research on this topic could provide added insight into the physical meaning behind the power law coefficient appearing in Jonscher's universal permittivity power law.

## References

- [1] M.-F. Yu, O. Lourie, M. J. Dyer, K. Moloni, T. F. Kelly, and R. S. Ruoff, *Science*, 287:637-640, 2000.
- [2] Sung-Hoon Park, Paul Theilmann, Peter Asbeck, and Prabhakar Bandaru, *Applied Physics Letters*, 94:243111-1, 2009.
- [3] Basudev Pradhan, et al., *Nano Letters*, 8(4):1142 – 1146, 2008.
- [4] S. Pfeifer, S.-H. Park, and Prabhakar Bandaru, *Journal of Applied Physics*, 108:024305-1 – 024305-4, 2010.
- [5] J. Keith Nelson [ed], *Dielectric Polymer Nanocomposites*, Springer Science+Business Media, LLC, New York, pp. 324–328, 2010.
- [6] P. Murugaraj, D. Mainwaring, and N. Mora-Huertas, “Dielectric enhancement in polymer-nanoparticle composites through interphase polarizability”, *Journal of Applied Physics*, 98:054304, 2005.
- [7] M. Roy, J. Nelson, R. MacCrone, and L. Schadler, “Polymer Nanocomposite Dielectrics – the Role of the Interface”, *IEEE Transactions Dielectric Insulation and Electrical Insulation*, 12(4):629 – 643, 2005.
- [8] Figure 1-1 is based on figure 1.2 in J. Keith Nelson [ed], *Dielectric Polymer Nanocomposites*, Springer Science+Business Media, LLC, New York, p. 5, 2010.
- [9] I. Balberg, C. Anderson, S. Alexander and N. Wagner, “Excluded volume and its relation to the onset of percolation”, *Physical Review B*, 30(7):3933 – 3943, 1984.
- [10] This figure is copied from figure 32 in J. Wernik and S. Meguid, “Recent Developments in Multifunctional Nanocomposites Using Carbon Nanotubes”, *Applied Mechanics Review*, 63:050801-1 - 050801-40, 2010.

- [11] Cover TM and Thomas JA., *Elements of Information Theory*. Hoboken, NJ: Wiley-Interscience, pp. 144 – 181, 2006.
- [12] Jean-Baptiste Jorcin, Mark. E. Orazem, Nadine Pebere, and Bernard Tribollet, *Electrochimica Acta*, 51:1473 – 1479, 2006.
- [13] P. Almond and B. Vainas, *J. Phys.: Condens. Matter*, 11: 9081 – 9093, 1999.
- [14] B. Vianas, D. P. Almond, J. Luo, and R. Stevens, *Solid State Ionics*, 126:65 – 80, 1999.
- [15] S. Kumar, N. Pimparkar, J. Y. Murthy, and M. A. Alam, *Applied Physics Letters*, 88:123505, 2007.
- [16] P. Hu, A. Fasoli, J. Park, Y. Choi, P. Estrela, S. L. Maeng, W. I. Milne, and A. C. Ferrari, *Journal of Applied Physics*, 104:074310-5, 2008.
- [17] S.-H. Park, P. Thielemann, P. Asbeck, and P. R. Bandaru, *IEEE Transactions of Nanotechnology*, 2009.
- [18] M. Ishida and F. Nihey, *Applied Physics Letters*, 92:163507, 2008.
- [19] I. Balberg, C. H. Anderson, S. Alexander, and N. Wagner, *Physical Review B*, 30:3933-3943, 1984.
- [20] I. Balberg, *Physical Review B*, 31:4053-4055, 1985.
- [21] L. Onsager, *Annals of the New York Academy of Sciences*, 51:627-659, 1949.
- [22] M.-F. Yu, O. Lourie, M. J. Dyer, K. Moloni, T. F. Kelly, and R. S. Ruoff, *Science*, 287:637-640, 2000.

[23] N. Li, Y. Huang, F. Du, X. He, X. Lin, H. Gao, Y. Ma, F. Li, Y. Chen, and P. C. Eklund, *Nanoletters*, 6:1141-1145, 2006.

[24] S.-H. Park, P. Thielemann, P. Asbeck, and P. R. Bandaru, *Applied Physics Letters*, 94:243111, 2009.

[25] S. J. Kang, C. Kocabas, T. Ozel, M. Shim, N. Pimparkar, M. A. Alam, S. V. Rotkin, and J. A. Rogers, *Nature Nanotechnology*, 2:230-236, 2007.

[26] J. Freund, *Modern Elementary Statistics*, (Prentice-Hall, New Jersey, 1979).

[27] S. Antonioti, S. Antonczak, and J. Golebiowski, *Theoretical Chemistry Accounts*, 112:290-297, 2004.

[28] J. Nichols, C. P. Deck, H. Saito, and P. R. Bandaru, *Journal of Applied Physics*, 102:064306, 2007.

[29] Sung-Hoon Park, Paul Theilmann, Peter Asbeck, and Prabhakar Bandaru, *Applied Physics Letters*, 94:243111-1, 2009.

[30] S.-H. Park, P. Thielemann, P. Asbeck, and P. R. Bandaru, *IEEE Transactions of Nanotechnology*, 2009.

[31] R. Abernethy, *The New Weibull Handbook*, (Robert B. Abernethy, North Palm Beach, FL, 2003).

[32] M.-F. Yu, O. Lourie, M. J. Dyer, K. Moloni, T. F. Kelly, and R. S. Ruoff, *Science*, 287:637-640, 2000.

[33] M.-F. Yu, O. Lourie, M. J. Dyer, K. Moloni, T. F. Kelly, and R. S. Ruoff, *Science*, 287:637-640, 2000.

- [34] R. Abernethy, *The New Weibull Handbook*, (Robert B. Abernethy, North Palm Beach, FL, 2003.
- [35] S. Kirkpatrick, *Reviews of Modern Physics*, 45: 574-588, 1973.
- [36] Ajayan P. M., Schadler L. S., Giannaris C. and Rubio A., "Single-Walled Carbon Nanotube-Polymer Composites: Strength and Weakness", *Advanced Materials*, 12:750-3, 2000.
- [37] Moniruzzaman M. and Winey K. I., "Polymer nanocomposites containing carbon nanotubes", *Macromolecules*, 39:5194-205, 2006.
- [38] Park S-H, Theilmann P., Asbeck P. and Bandaru P. R., "Enhanced electromagnetic interference shielding through the use of functionalized carbon nanotube-reactive polymer composites", *IEEE Transactions of Nanotechnology*, 9:464-9, 2010.
- [39] Park S-H, Theilmann P., Asbeck P. and Bandaru P. R., "Enhanced dielectric constants and shielding effectiveness of, uniformly dispersed, functionalized carbon nanotube composites", *Applied Physics Letters*, 94:243111, 2009.
- [40] Chung D. D. L. "Electromagnetic Interference Shielding Effectiveness of Carbon Materials", *Carbon*, 39:279-85, 2001.
- [41] Pradhan B., Setyowati K., Liu H., Waldeck D. H. and Chen J., "Carbon nanotube-polymer nanocomposite infrared sensor", *Nanoletters*, 8:1142-6, 2008.
- [42] Bekyarova E., Thostenson E. T., Yu A., Itkis M. E., Fakhrutdinov D., Chou T-W and Haddon R. C., "Functionalized single-walled carbon nanotubes for carbon fiber-epoxy composites", *Journal of Physical Chemistry C*, 111:17865-71, 2007.
- [43] Park S-H and Bandaru P. R., "Improved mechanical properties of carbon nanotube/polymer composites through the use of carboxyl-epoxide functional group linkages", *Polymer*, 51:5071-7, 2010.

- [44] Breuer O. and Sundararaj U. “Big returns from small fibers: A review of polymer/carbon nanotube composites”, *Polymer Composites*, 25:630-45, 2004.
- [45] Todd M. G. and Shi F. G., “Complex permittivity of composite systems: a comprehensive interphase approach”, *IEEE Transactions on Dielectrics and Electrical Insulation*, 12:601-11, 2005.
- [46] Smith R. C., Liang C., Landry M., Nelson J. K. and Schadler L. S., “The Mechanisms Leading to the Useful Electrical Properties of Polymer Nanodielectrics”, *IEEE Transactions on Dielectrics and Electrical Insulation*, 15:187-96, 2008.
- [47] Fiedler B., Gojny F. H., Wichmann M. H. G., Nolte M. C. M. and Schulte K., “Fundamental aspects of nano-reinforced composites”, *Composites Science and Technology*, 66:3115-25, 2006.
- [48] Lee L. J., Zeng C., Cao X., Han X., Shen J. and Xu G., “Polymer nanocomposite foams”, *Composites Science and Technology*, 65 2344-63, 2005.
- [49] Kim K. H. and Jo W. H., “A strategy for enhancement of mechanical and electrical properties of polycarbonate/multi-walled carbon nanotube composites”, *Carbon*, 47:1126-34, 2009.
- [50] Yeh M. K., Tai N. H. and Lin Y. J., “Mechanical properties of phenolic-based nanocomposites reinforced by multi-walled carbon nanotubes and carbon fibers”, *Composites, Part A*, 39 677-84, 2008.
- [51] Lo’pez Manchado M. A., Valentini L., Biagiotti J. and Kenny J. M., “Thermal and mechanical properties of single-walled carbon nanotubes–polypropylene composites prepared by melt processing”, *Carbon*, 43:1499-505, 2005.
- [52] Tai N. H., Yeh M. K. and Peng T. H., “Experimental study and theoretical analysis on the mechanical properties of SWNTs/phenolic composites”, *Composites B*, 39:926-32, 2008.

[53] Lo'pez Manchado M. A., Valentini L., Biagiotti J. and Kenny J. M., "Thermal and mechanical properties of single-walled carbon nanotubes–polypropylene composites prepared by melt processing", *Carbon*, 43:1499-505, 2005.

[54] Park S-H and Bandaru P. R., "Improved mechanical properties of carbon nanotube/polymer composites through the use of carboxyl-epoxide functional group linkages", *Polymer*, 51:5071-7, 2010.

[55] Park S-H, Theilmann P., Asbeck P. and Bandaru P. R., "Enhanced electromagnetic interference shielding through the use of functionalized carbon nanotube-reactive polymer composites", *IEEE Transactions of Nanotechnology*, 9:464-9, 2010.

[56] Tasis D., Tagmatarchis N., Bianco A. and Prato M., "Chemistry of Carbon Nanotubes", *Chemical Reviews*, 106:1105-35, 2006.

[57] Pfeifer S., Park S-H and Bandaru P. R., "Analysis of electrical percolation thresholds in carbon nanotube networks using the Weibull probability distribution", *Journal of Applied Physics*, 108:024305, 2010.

[58] Rogers A., *Statistical analysis of spatial dispersion – the quadrat method*, (London, UK: Pion Ltd.), 1974.

[59] Kim D., Lee J. S., Barry C. M. F. and Mead J. L., "Microscopic measurement of the degree of mixing for nanoparticles in polymer nanocomposites by TEM images", *Microscopy Research and Technique*, 70:539-46, 2007.

[60] Cover T. M. and Thomas J. A., *Elements of Information Theory* (Hoboken, NJ: Wiley-Interscience) 2006.

[61] Cencov N. N., *Statistical Decision Rules and Optimal Inference*, vol 53 (Providence, RI: American Mathematical Society) 1982.

[62] Dabak A. G., *A Geometry for Detection Theory*. In: Department of Electrical and Computer Engineering, (Houston, TX: Rice University) 1992.

[63] Cover T. M. and Thomas J. A., *Elements of Information Theory* (Hoboken, NJ: Wiley-Interscience) 2006.

[64] Johnson D. and Sinanovic S., “Symmetrizing the Kullback-Leibler distance” (Houston, TX: Rice University) 2001.

[65] Rogers A., *Statistical analysis of spatial dispersion – the quadrat method*, (London, UK: Pion Ltd.), 1974.

[66] Feng D. and Jin G., *Introduction to Condensed Matter Physics*, (Singapore: World Scientific Publishing Co. plc. Ltd) 2005.

[67] Gonzalez R. C. and Woods R. E., *Digital Image Processing*, (Upper Saddle River, NJ: Prentice-Hall, Inc.,) 2002.

[68] Kim D., Lee J. S., Barry C. M. F. and Mead J. L., “Microscopic measurement of the degree of mixing for nanoparticles in polymer nanocomposites by TEM images”, *Microscopy Research and Technique*, 70:539-46, 2007.

[69] Khare H. S. and Burriss D. L. “A quantitative method for measuring nanocomposite dispersion”, *Polymer*, 51:719-29, 2010.

[70] Kim D., Lee J. S., Barry C. M. F. and Mead J. L., “Microscopic measurement of the degree of mixing for nanoparticles in polymer nanocomposites by TEM images”, *Microscopy Research and Technique*, 70:539-46, 2007.

[71] Tasis D., Tagmatarchis N., Bianco A. and Prato M., “Chemistry of Carbon Nanotubes”, *Chemical Reviews*, 106:1105-35, 2006.

[72] Love C. T., Gapin A. and Karbhari V. M., “Interfacial Adhesion in Multi-Walled Carbon Nanotube/Reactive Ethylene Terpolymer Composites”, In: *Society for the Advancement of Material and Process Engineering (SAMPE)*, (Baltimore, MD) 2007.

[73] Love C. T., Gapin A. and Karbhari V. M., “Multi-Walled Carbon Nanotube Reactive Thermoplastic Composite Adhesives”, In: *1st International Conference on Nanopolymers*, (Berlin, Germany) 2007.

[74] Bandaru P. R., Daraio C., Yang K. and Rao A. M., “A plausible mechanism for the evolution of helical forms in nanostructure growth”, *Journal of Applied Physics*, 101:094307, 2007.

[75] Wang W., Yang K., Gaillard J., Bandaru P. R. and Rao A. M., “Rational synthesis of helically coiled carbon nanowires and nanotubes through the use of Tin and Indium catalysts”, *Advanced Materials*, 20:179-82, 2008.

[76] Park S-H, Theilmann P., Asbeck P. and Bandaru P. R., “Enhanced electromagnetic interference shielding through the use of functionalized carbon nanotube-reactive polymer composites”, *IEEE Transactions of Nanotechnology*, 9:464-9, 2010.

[77] Park S-H, Theilmann P., Asbeck P. and Bandaru P. R., “Enhanced dielectric constants and shielding effectiveness of, uniformly dispersed, functionalized carbon nanotube composites”, *Applied Physics Letters*, 94:243111, 2009.

[78] Park S-H and Bandaru P. R., “Improved mechanical properties of carbon nanotube/polymer composites through the use of carboxyl-epoxide functional group linkages”, *Polymer*, 51:5071-7, 2010.

[79] Sun L., Warren G. L., O'Reilly J. Y., Everett W. N., Lee S. M., Davis D., Lagoudas D. and Sue H-J, “Mechanical properties of surface-functionalized SWCNT/epoxy composites”, *Carbon*, 2008;46:320-28, 2008.

- [80] Park S-H, Theilmann P., Asbeck P. and Bandaru P. R., “Enhanced electromagnetic interference shielding through the use of functionalized carbon nanotube-reactive polymer composites”, *IEEE Transactions of Nanotechnology*, 2009.
- [81] Cover T. M. and Thomas J. A., *Elements of Information Theory* (Hoboken, NJ: Wiley-Interscience) 2006.
- [82] Khare H. S. and Burriss D. L. “A quantitative method for measuring nanocomposite dispersion”, *Polymer*, 51:719-29, 2010.
- [83] Kim D., Lee J. S., Barry C. M. F. and Mead J. L., “Microscopic measurement of the degree of mixing for nanoparticles in polymer nanocomposites by TEM images”, *Microscopy Research and Technique*, 70:539-46, 2007.
- [84] Khare H. S. and Burriss D. L. “A quantitative method for measuring nanocomposite dispersion”, *Polymer*, 51:719-29, 2010.
- [85] Khare H. S. and Burriss D. L. “A quantitative method for measuring nanocomposite dispersion”, *Polymer*, 51:719-29, 2010.
- [86] Kim D., Lee J. S., Barry C. M. F. and Mead J. L., “Microscopic measurement of the degree of mixing for nanoparticles in polymer nanocomposites by TEM images”, *Microscopy Research and Technique*, 70:539-46, 2007.
- [87] Chambers D. S. and Wheeler D. J., Understanding statistical process control, (Knoxville, TN: SPC Press) 1992.
- [88] S. Pfeifer, S. H. Park, and P. R. Bandaru, *Journal of Applied Physics*, 108, 024305 (2010).
- [89] D. D. L. Chung, *Carbon*, 39, 279-285 (2001).
- [90] M. J. Biercuk, M. C. Llaguno, M. Radosavljevic, J. K. Hyun, A. T. Johnson, and J. E. Fischer, *Applied Physics Letters*, 80, 2767-2769 (2002).

- [91] M. Hughes, in Dekker, Encyclopedia of Nanoscience and Nanotechnology (Taylor & Francis, London, 2004), p. 447-459.
- [92] E. S. A. Rashid, K. Ariffin, H. M. Akil, and C. C. Kooi, *Journal of Reinforced Plastics and Composites*, 27, 1573-1584 (2008).
- [93] M. G. Todd and F. G. Shi, *IEEE Transactions on Dielectrics and Electrical Insulation*, 12, 601-611 (2005).
- [94] S.-H. Park, P. Thielemann, P. Asbeck, and P. R. Bandaru, *Applied Physics Letters*, 94, 243111 (2009).
- [95] S.-H. Park, P. Theilmann, P. Asbeck, and P. R. Bandaru, *IEEE Transactions of Nanotechnology*, 9, 464-469 (2010).
- [96] D. Tasis, N. Tagmatarchis, A. Bianco, and M. Prato, *Chemical Reviews*, 106, 1105-1135 (2006).
- [97] S.-H. Park, P. Theilmann, P. Asbeck, and P. R. Bandaru, *IEEE Transactions of Nanotechnology*, 9, 464-469 (2010).
- [98] S. Pfeifer and P. R. Bandaru, *Nanotechnology* (in press) (2012).
- [99] D. M. Pozar, *Microwave Engineering*, 2 ed. (John Wiley & Sons, Inc., New York, 1998).
- [100] C. R. Paul, Introduction to Electromagnetic Compatibility, 2 ed. (Wiley-Interscience, New York, NY, 2006).
- [101] D. P. Almond, C. R. Bowen, and D. A. S. Rees, *Journal of Physics D: Applied Physics*, 39, 1295-1304 (2006).

- [102] J. Valsa and J. Vlach, *International Journal of Circuit Theory and Applications* DOI: 10.1002/cta.785 (2011).
- [103] B. Vianas, D. P. Almond, J. Luo, and R. Stevens, *Solid State Ionics*, 126, 65-80 (1999).
- [104] J.-B. Jorcin, M. E. Orazem, N. Pebere, and B. Tribollet, *Electrochimica Acta*, 51, 1473-1479 (2006).
- [105] E. Barsoukov and J. R. MacDonald, Impedance Spectroscopy: Theory, Experiment, and Applications (Wiley-Interscience, Hoboken, NJ, 2005).
- [106] J.-B. Jorcin, M. E. Orazem, N. Pebere, and B. Tribollet, *Electrochimica Acta*, 51, 1473-1479 (2006).
- [107] D. S. Chambers and D. J. Wheeler, Understanding statistical process control 2ed. (SPC Press, Knoxville, TN, 1992).
- [108] A. D. R. McQuarrie and C.-L. Tsai, Regression and Time Series Model Selection (World Scientific., 1998).
- [109] M. G. Todd and F. G. Shi, *IEEE Transactions on Dielectrics and Electrical Insulation*, 12, 601-611 (2005).
- [110] L. Jylha and A. Sihvola, *Journal of Physics D: Applied Physics*, 40, 4966-4973 (2007).
- [111] L. Wang and Z. Dang, *Applied Physics Letters*, 87, 042903 (2005).
- [112] Morris Cohen [ed.], *Quantitative Stereology*, Addison-Wesley Publishing Company, Inc., Reading, Massachusetts, pp. 25 – 27, 1970.

[113] D. P. Almond, C. R. Bowen, and D. A. S. Rees, "Composite dielectrics and conductors: simulation, characterization and design", *Journal of Physics D: Applied Physics*, 39:1299, 2006.